A high-resolution sequence stratigraphic framework for the eastern Ellis Bay Formation, Canada: A record of Hirnantian sea-level change

Joshua B. Zimmt[1,2,†], Steven M. Holland[3], André Desrochers[4], David S. Jones[5], and Seth Finnegan[1]

[1]*University of California Museum of Paleontology and Department of Integrative Biology, University of California, Berkeley, 1101 Valley Life Science Building, Berkeley, California 94720, USA*

[2]*Department of Earth and Planetary Sciences, McGill University, 3450 University Street, Montreal, Quebec H3A 0E8, Canada*

[3]*Department of Geology, University of Georgia, 210 Field Street, Athens, Georgia 30602, USA*

[4]*Department of Earth and Environmental Sciences, University of Ottawa, 150 Louis-Pasteur Private, Room 342, Ottawa, Ontario K1N 6N5, Canada*

[5]*Department of Geology, Amherst College, 11 Barrett Hill Road, Amherst, Massachusetts 01002, USA*

ABSTRACT

Anticosti Island (Québec, Canada) contains one of the thickest Ordovician/Silurian boundary sections in the world, providing a fossiliferous and well-preserved record of the Late Ordovician mass extinction; however, the absence of a comprehensive correlation framework for the island prevents the full incorporation of data from across Anticosti into a global understanding of the extinction event. Here, we combine sedimentological, stratigraphic, and chemostratigraphic data to develop a sequence stratigraphic framework for the Ellis Bay and lowermost Becscie formations along the northeastern shore of Anticosti Island. These formations record six fourth-order (∼100–400 k.y.) depositional sequences bounded by regionally traceable unconformities. Evidence of subaerial weathering and exposure at many of these unconformities is subtle and has long gone unrecognized, which highlights the complexity of correlation in this and other stratigraphically thin icehouse records. Quartz pebble lags that mantle these surfaces punctuate the otherwise fine-grained, mixed carbonate–siliciclastic strata of the Ellis Bay Formation and provide the means to trace unconformities across localities; these surfaces are also marked by depleted carbon isotopic values, meteoric cement, microkarst, and incised valleys. This sequence stratigraphic framework provides the first correlation framework for exposures from the eastern end of this classic Ordovician/Silurian boundary section, and thus enables the integration of paleobiological, stratigraphic, and geochemical data into a basin-wide perspective of the Late Ordovician mass extinction. Critically, comparison to sequence stratigraphic frameworks from coeval sections suggests that other regions may be incomplete at the level of the fourth-order cycles recorded on Anticosti Island and may contain similarly cryptic unconformities.

INTRODUCTION

The end of the Ordovician Period was marked by a series of major climatic (e.g., Brenchley et al., 1994; Goldberg et al., 2021), oceanographic (e.g., Pohl et al., 2016; Bartlett et al., 2018), and biotic events (e.g., Finnegan et al., 2012; Harper et al., 2014; Rong et al., 2020) as the early Paleozoic Icehouse (Page et al., 2007; ca. 470–425 Ma) reached its acme. As the icehouse waxed at the start of the latest Ordovician Hirnantian Stage (445.21–443.07 Ma), continental ice sheets rapidly expanded over high southern latitudes, ushering in an interval marked by glacioeustatic sea-level fluctuations exceeding that of the Last Glacial Maximum (Finnegan et al., 2011), a cooling of tropical sea-surface temperatures (Vandenbroucke et al., 2010), and global changes in oceanic redox conditions (Bartlett et al., 2018; Zou et al., 2018). Together, these consequences of the glaciation are often cited as triggering the Late Ordovician mass extinction, which drove ∼80% of marine species to extinction (Sheehan, 2001). An accurate sequencing of Hirnantian events is critical for interpreting the causal relationship between the Late Ordovician mass extinction and potential climate-related drivers. However, global syntheses of Hirnantian records at the substage level offer conflicting interpretations of the sequence of events across the Ordovician/Silurian boundary and their relationship to the mass extinction (e.g., Sheehan, 2001; Harper et al., 2014; Wang et al., 2019; Rong et al., 2020). In part, this is due to the short duration (∼2 m.y. or shorter; Goldman et al., 2020) of the Hirnantian Stage and the limitations of biostratigraphic and chemostratigraphic correlation schemes that are used to align stratigraphic records among sedimentary basins (Dowsett, 1988; Rong et al., 2002; Xiao et al., 2018; see Jones et al., 2020).

A regional, basin-wide assessment of the Ordovician/Silurian boundary could provide a detailed perspective on the timing of oceanographic and climatic events during the early Paleozoic Icehouse and their relationship to the Late Ordovician mass extinction. The peak of the early Paleozoic Icehouse, like those of other icehouse climates, was characterized by major glacioeustatic fluctuations that produced complex stratigraphic architecture in marine basins. Hirnantian exposures are marked by abrupt facies shifts and subaerial unconformities that record large changes in relative sea level (Moreau, 2011; Ghienne et al., 2014; Kiipli and Kiipli, 2020; Calner et al., 2021). This complicates the sequencing of events during the Late Ordovician mass extinction, as stratigraphic architecture is an overarching control on the expression and preservation of biotic events in the fossil record (Holland and Patzkowsky, 2015; Holland, 2020). Properly interpreting the sequence of events during the Hirnantian and their relationship to the mass extinction hinges on an accurate understanding of the structure of the stratigraphic record. Sequence stratigraphic principles provide a framework for combining data from individual stratigraphic columns across a basin into a comprehensive understanding of the pattern and drivers of mass extinctions (Holland and Patzkowsky, 2015; Zimmt et al., 2021). This makes

Joshua B. Zimmt https://orcid.org/0000-0002-3960-283X
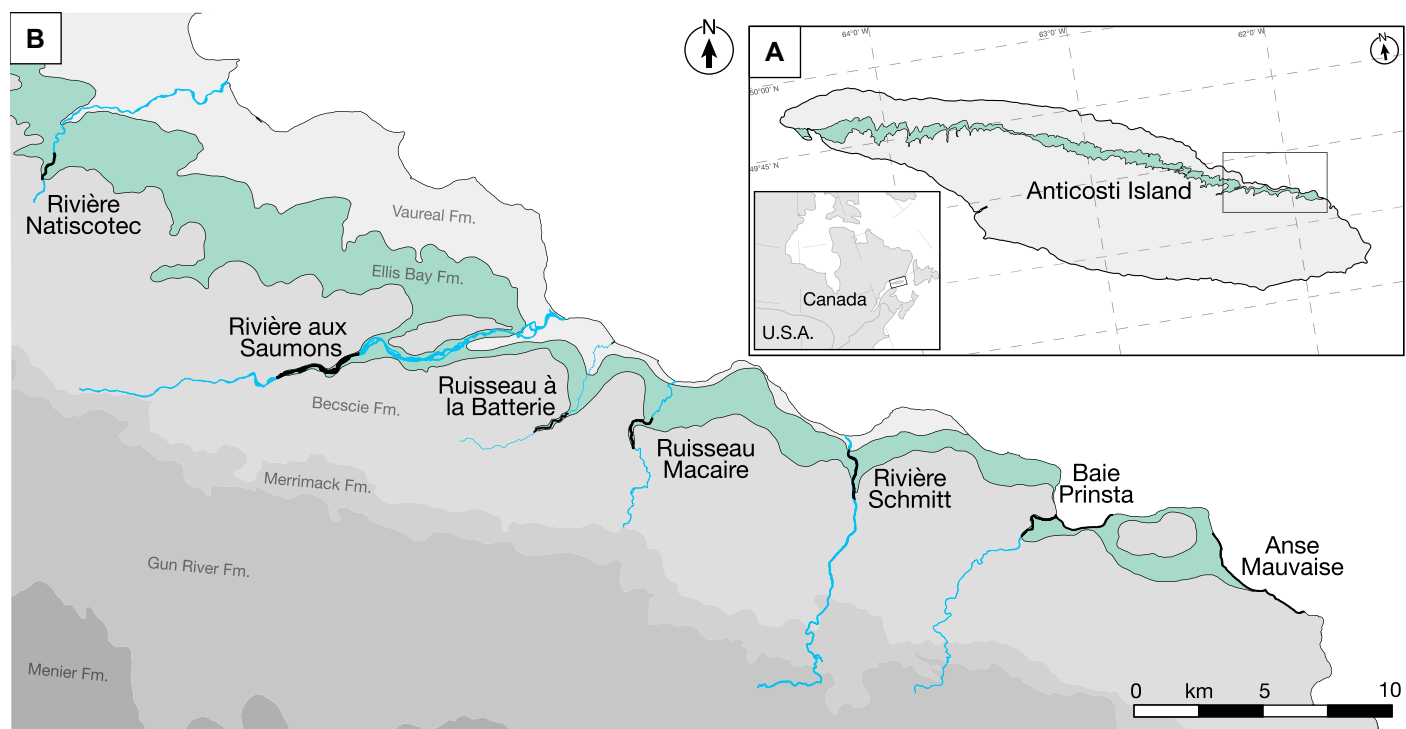†josh_zimmt@berkeley.edu

Figure 1. Regional and local context of the study area on Anticosti Island (Québec, Canada). (A) Regional context of Anticosti Island in eastern Canada (inset; black box) depicting the mapped extent of the Ellis Bay Formation, shaded in green. (B) Measured stratigraphic columns (black lines) of the Ellis Bay Formation along the eastern end of Anticosti Island. Ordovician/Silurian boundary exposures include Rivière Natiscotec (49.47217°N, 62.51543°W), Rivière aux Saumons (49.39915°N, 62.36715°W), Ruisseau à la Batterie (49.38298°N, 62.24535°W), Ruisseau Macaire (49.37915°N, 62.20415°W), Rivière Schmitt (49.36435°N, 62.08352°W), Baie Prinsta (49.34463°N, 61.96760°W), and Anse Mauvaise (49.32336°N, 61.86337°W). Given coordinates reflect the midpoint of each exposure. Geologic map data are from Desrochers and Gauthier (2009); note that the lower boundary of the Ellis Bay Formation on this map is based on the definition of the Ellis Bay Formation sensu Long and Copper (1987a) and therefore does not correspond to the formational boundary of the Ellis Bay Formation as defined in this paper (see Copper et al., 2013).

a sequence stratigraphic perspective critical for interpreting regional records of the Hirnantian Stage and thus the pattern and drivers of the Late Ordovician mass extinction.

Here, we develop a sequence stratigraphic framework for the eastern Ellis Bay (Hirnantian) and lowermost Becscie (Hirnantian/Rhuddanian) formations along the northeastern shore of Anticosti Island (Québec, Canada; Fig. 1). Careful study of the stratigraphic record from a sequence-stratigraphic perspective enables the recognition of cryptic unconformities that bound six depositional sequences within the eastern Ellis Bay Formation. Many of these unconformities are unrecognizable in outcrop but are mantled by conspicuous horizons of quartz pebbles that can be traced across the study area. The presence of these quartz pebble lags in the otherwise fine-grained, carbonate-siliciclastic strata of the eastern Ellis Bay Formation signifies a major fall in relative sea level that exposed portions of the ramp to subaerial weathering and erosion. The recognition of these six sequences solves the long-standing issue of correlation

across the eastern Ellis Bay Formation and for the first time provides a correlation framework for the far end of this classic Ordovician/Silurian boundary section. Eastern exposures of the Ellis Bay Formation, long understood to be crucial sources of paleobiological, geochemical, and stratigraphic data, can now be incorporated into comprehensive studies of the Hirnantian Stage on Anticosti Island. We discuss the implications of this new framework for understanding the sequence of climatic, oceanographic, and biotic events across the Ordovician/Silurian boundary.

BACKGROUND

Strata exposed on Anticosti Island (Québec, Canada) preserve the Upper Ordovician and lower Silurian succession of the Anticosti Basin, a foreland basin that constitutes the eastern segment of the St. Lawrence Platform (Sanford, 1993). In the northern part of the basin around Anticosti Island, the Anticosti Basin corresponds to an undeformed homoclinal ramp that gently dips to the southwest (Castonguay et al., 2005). To the

north, the sedimentary succession of the Anticosti Basin onlaps the Grenvillian metamorphic rocks of the Canadian Shield, and to the south, the basin is bounded by a fold-and-thrust belt that formed over successive Appalachian orogenies (Pinet and Lavoie, 2007). Subsidence rates associated with early Paleozoic thrust loading apparently peaked with the emplacement of Taconic thrust sheets in the Gaspé area during the Late Ordovician and diminished across the Ordovician/Silurian boundary as the basin transitioned to a successor basin (Long, 2007). Situated north of this Taconic deformation front, the succession on Anticosti Island is relatively undeformed despite the long-lived tectonic history of the basin (Pinet et al., 2012). Reflection seismic profiles show that minor normal faults, which played an important role in the Late Ordovician accommodation history of the basin, affected only subsurface strata on Anticosti Island (Bordet et al., 2010).

During latest Ordovician and earliest Silurian times, the Anticosti Basin was located along the eastern margin of Laurentia between 0° and 30°S paleolatitude (Fig. 2; McLaughlin and Brett,
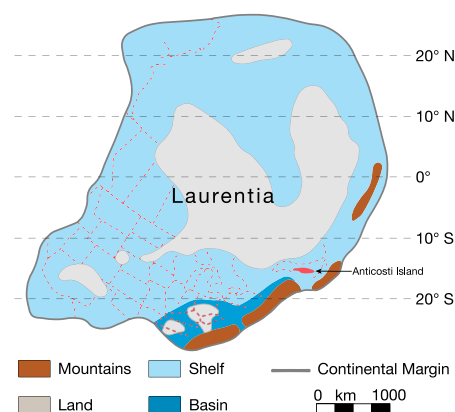
Figure 2. Paleogeographic reconstruction of Laurentia depicting one reconstruction of the approximate paleolatitude of Anticosti Island during the Late Ordovician (adapted from McLaughlin and Brett, 2007).

2007; Torsvik and Cocks, 2016; Cocks and Torsvik, 2021; Swanson-Hysell and Macdonald, 2017). Sedimentation along the shallow ramp was dominated by storm processes, reflecting the position of Anticosti Island within the tropical storm belt (Sami and Desrochers, 1992; Long, 2007). This thick (~900 m) stratigraphic succession is exposed in an east–west-trending outcrop belt across the 200 km length of Anticosti Island and is divided into eight formations that span the Ordovician/Silurian boundary (Fig. 2; Schuchert and Twehhofel, 1910; Copper and Long, 1988; Copper et al., 2012; Copper and Jin, 2014, 2015), with the Ordovician portion of the succession comprising the Vaureal and Ellis Bay formations.

The Upper Ordovician Ellis Bay Formation preserves a succession of mixed carbonate–siliciclastic facies. In the east, the formation consists of a succession of shallow-water, mixed carbonate–siliciclastic facies, while in the west, the Ellis Bay Formation consists of a suite of deeper-water, predominantly carbonate and shale-dominated facies (Petryk, 1981; Long and Copper, 1987a; Desrochers et al., 2010), which is consistent with the southwestern depositional dip of the ramp. Here, we distinguish between the western and eastern Ellis Bay Formation sensu Copper et al. (2013) to highlight their lithologic differences. Uncertainties in the lateral transition between these facies suites and poor exposure of the Ellis Bay Formation in the center of the island have complicated the development of a correlation framework for the formation. Long and Copper (1987a) were the first to propose an east–west correlation framework between the westernmost (Anse aux Fraises to Pointe Laframboise) and easternmost (Anse Mauvaise) exposures of the Ellis Bay Formation (Fig. 1),

dividing the Ellis Bay Formation at Anse Mauvaise into five members (Grindstone, Velleda, Prinsta, Lousy Cove, and Laframboise), which they tentatively correlated with Bolton's (1972) lithostratigraphic framework for the Ellis Bay Formation based on exposures from the western coast of the island. Later, Copper (2001) formally extended the lithostratigraphic framework of Long and Copper (1987a) to the western exposures of the Ellis Bay Formation.

An assessment of chitinozoan assemblages from Upper Ordovician and lower Silurian strata on Anticosti Island by Achab et al. (2011, 2013) revealed that the base of the Ellis Bay Formation as established by Copper (2001) is highly diachronous. Building upon the biostratigraphic framework established by Achab et al. (2011, 2013), Desrochers et al. (2010) described five transgressive–regressive (T–R) cycles for the Ellis Bay Formation. Copper et al. (2013) subsequently attempted to reconcile these lithostratigraphic and sequence stratigraphic frameworks by proposing separate lithostratigraphic frameworks for the western and eastern exposures of the Ellis Bay Formation. In the west, Copper et al. (2013) divided the Ellis Bay Formation into the Fraise, Juncliff, Parastro, Lousy Cove, and Laframboise members. In the east, they retained the nomenclature of Long and Copper (1987a) but placed the boundary of the Ellis Bay Formation at the base of the Prinsta Member. This established two parallel sequence stratigraphic (Desrochers et al., 2010) and lithostratigraphic (Copper et al., 2013) frameworks for correlation within the Ellis Bay Formation, both of which relied on biostratigraphic constraints to define the Ellis Bay Formation. However, the applicability of a sequence stratigraphic framework that spans all western and eastern exposures of the Ellis Bay Formation has yet to be tested, hindering the integration of paleontological and geochemical data from Anticosti into a regional understanding of the Late Ordovician mass extinction.

Several lines of evidence support a Hirnantian age for the Ellis Bay Formation (Copper et al., 2013). These include the occurrences of the brachiopods *Hirnantia* (Jin and Zhan, 2008; Zimmt and Jin, 2023) in the lowermost eastern Ellis Bay Formation and *Hindella* (Copper and Jin, 2017) in the lowermost western Ellis Bay Formation. The post-Richmondian conodont Fauna 13, which is used to define the Gamachian Stage—the regional equivalent to the Hirnantian Stage (Twehhofel et al., 1954; Goldman et al., 2020)—also first appears at the base of the western Ellis Bay Formation (McCracken and Barnes, 1981; McCracken and Nowlan, 1988) and likewise supports a Hirnantian age (Goldman et al., 2020). Higher in the formation, diagnostic graptolites from the *Metabolograptus persculptus*

Zone (Melchin, 2008) and Hirnantian chitinozoans (Achab et al., 2011, 2013) occur within the Lousy Cove and Laframboise members, which affirms a Hirnantian age for the entire Ellis Bay Formation.

The position of the Ordovician/Silurian system boundary on Anticosti Island is uncertain. Across the Ellis Bay/Becscie contact, brachiopod (Jin and Zhan, 2008; Li and Copper, 2006), chitinozoan (Achab et al., 2011, 2013), conodont (McCracken and Barnes, 1981; McCracken and Nowlan, 1988), and graptolite (Melchin, 2008) faunas transition to assemblages with latest Hirnantian to earliest Silurian affinities. These changes suggest that the system boundary lies at the Ellis Bay/Becscie contact or within the lowermost Becscie Formation (Petryk, 1981; Long and Copper, 1987a; Desrochers et al., 2010), but the precise position remains unclear.

METHODS

Seven closely spaced exposures of the uppermost Vaureal, Ellis Bay, and lowermost Becscie formations were measured along the northeastern coast of Anticosti Island (Figs. 1 and 3). Lithostratigraphic nomenclature for members and formations, unless otherwise specified, follows Copper et al. (2013). Note that west of Anse Mauvaise, the position of the Vaureal/Ellis Bay contact and lithostratigraphic units of the eastern Ellis Bay Formation, as described by Copper et al. (2013), are difficult to trace, with the exception of the Laframboise Member, which is marked at its base by a regional Oncolite Platform Bed sensu Desrochers et al. (2010). For each exposure, bedding thickness and character (Ingram, 1954), lithology, sedimentary structures, and body fossils were used to define facies. Thin sections for detailed lithological characterization were made of representative samples of each facies and at major stratigraphic contacts. Relationships among facies were inferred from regional correlations as well as gradational vertical facies transitions.

At each exposure, samples were collected for stable carbon and oxygen isotopic analyses at 0.5 m spacing through the Vaureal Formation, the sub-Laframboise Ellis Bay Formation, and the lowermost Becscie Formation. Sampling near the Laframboise Member was conducted at a spacing of 0.1–0.25 m. Samples were sectioned and polished to sample micrite and fine-grained carbonate, where available, to characterize trends in the isotopic composition of seawater within the Anticosti Basin. At the Center for Stable Isotope Biogeochemistry at the University of California, Berkeley, in Berkeley, California, USA, isotopic analyses were conducted using a fully automated MultiCarb GV
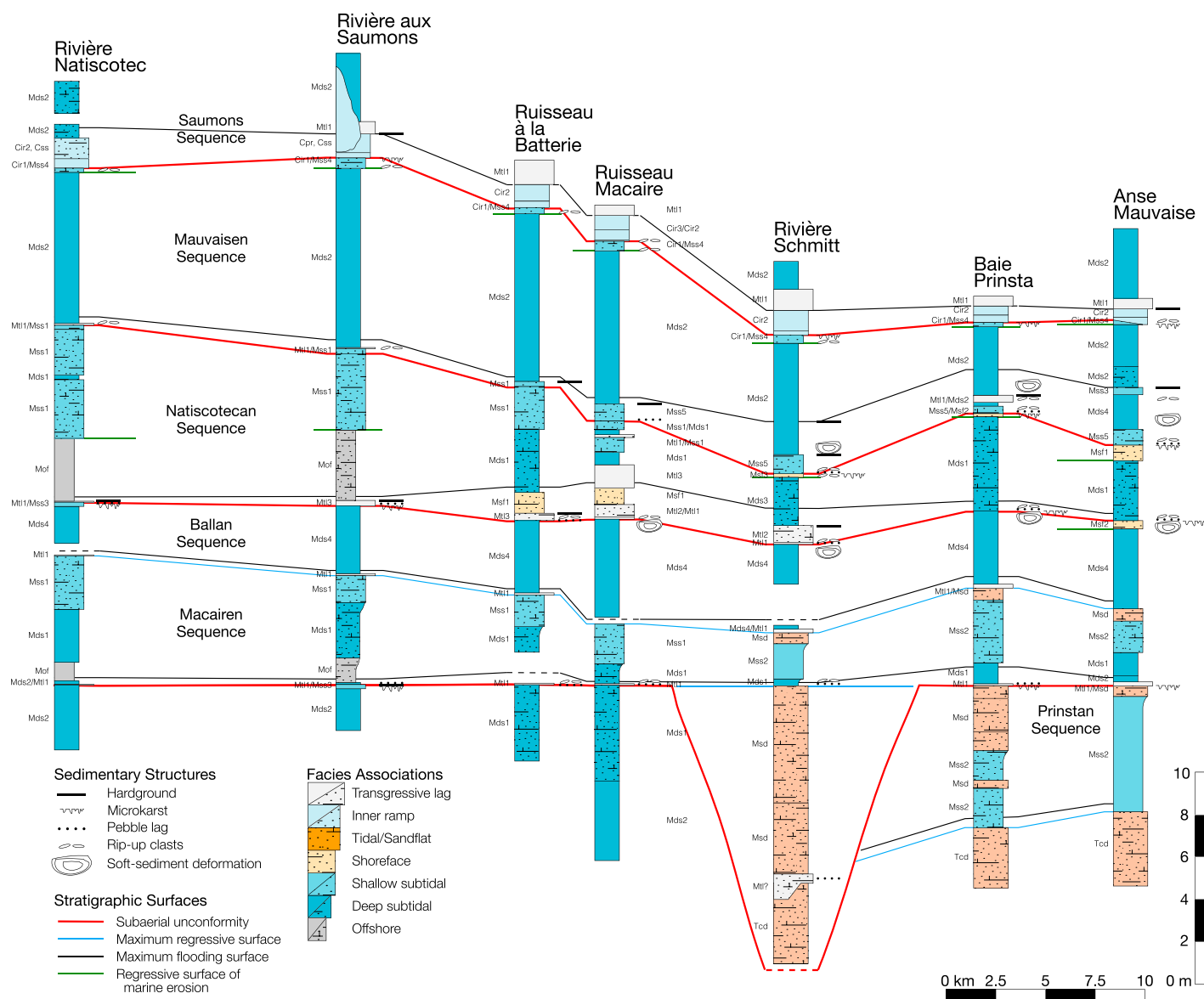
Figure 3. Sequence-stratigraphic cross section of the eastern Ellis Bay Formation, using the maximum regressive surface of the Macairen Sequence as a datum. Major stratigraphic surfaces, including sequence-bounding unconformities (marked in red and bolded), maximum regressive surfaces (marked in blue), and maximum flooding surfaces (marked in black), can be traced across the study area; regressive surfaces of marine erosion (marked in green) are indicated but cannot be traced across localities. Alphanumeric codes to the left of each stratigraphic column refer to the facies associations listed in Tables 1–3; alphanumeric codes separated by a slash indicate where one facies (right of slash) is overlain by another facies (left of slash) over a thin stratigraphic interval.

IsoPrime system operated in dual inlet mode. At the Stable Isotope Biogeochemistry Lab at Washington University in Saint Louis, Missouri, USA, isotopic analyses were conducted using a Thermo Scientific Gas Bench II coupled to a DELTA V Advantage mass spectrometer. All stable isotopic values are reported in parts per mil (‰) relative to the Vienna Peedee belemnite (VPDB) standard by correcting to NBS-19 standards used for each run. The average analytical precision across all runs at the Center for Stable Isotope Biogeochemistry is (1σ) ±0.05‰ for δ18O and ±0.07‰ for δ13C, and at Washington University in Saint Louis, it is ±0.22‰ for δ18O and ±0.07‰ for δ13C. New isotopic data are supplemented with previously published data from Jones et al. (2011). The full dataset can be found in the Supplemental Material[1].

FACIES ASSOCIATIONS AND DEPOSITIONAL SYSTEMS

Overview of Depositional Systems

Three depositional systems are recognized within the study area: the siliciclastic tidal (prefix T; Table 1), mixed carbonate–siliciclastic ramp (prefix M; Table 2), and carbonate ramp (prefix C; Table 3) depositional systems. Facies within the mixed carbonate–siliciclastic ramp and carbonate ramp depositional systems reflect

TABLE 1. SILICICLASTIC TIDAL DEPOSITIONAL SYSTEM

Facies association and interpretation	Lithology and bedding	Sedimentary structures	Taphonomy	Contacts and context
Tcd, compound dune	Very fine sandstone interbedded with mudstone, transitioning upward to very fine to coarse sandstone. Contains lags of angular mudstone clasts, coarse sand, and gastropods at the base of troughs.	Large-scale trough cross-bedding in sets 30–50 cm thick with tidal bundling, clay drapes, and coarse lags at the base of sets. Heterolithic cross-stratification; sigmoidal cross-stratification; flaser, wavy, and lenticular bedding; and herringbone cross-stratification.	Very rare tabulate corals, stromatoporoids, and aulacerids, both abraded and fragmented. Smaller marine fossils are commonly abraded and concentrated in lenses.	Present below base of the Prinstan Sequence in updip localities.

a dominant control of storm processes, which is consistent with the findings of previous studies (Sami and Desrochers, 1992), and some facies in these two systems also preserve evidence of tidal processes (Tables 2 and 3; Fig. 3). Both systems are present across the study area. The siliciclastic tidal system is unique in the study area for the dominance of tidal processes and in its restriction to depositionally updip (i.e., eastern) exposures (Fig. 3).

For each facies, an interpretation of key features is given in the text, with detailed descriptions provided in Tables 1–3. In some cases, interpretations of facies differ substantially from those of previous studies (e.g., Long and Copper, 1987a, 1987b; Desrochers et al., 2010).

Depositional Systems of the Eastern Ellis Bay and Uppermost Vaureal Formations

Siliciclastic Tidal Depositional System

The siliciclastic tidal depositional system contains a single siliciclastic facies association: the compound dune association (Table 1). It is present at the top of the Vaureal Formation (sensu Copper et al., 2013) at Baie Prinsta and Anse Mauvaise, as well as at Rivière Schmitt (Fig. 3).

The compound dune facies association (Tcd) consists of large-scale, trough cross-bedded sandstone with internal discontinuities at the base of foresets that are marked by angular mudstone (siliciclastic lithology) intraclasts, siliciclastic coarse sand and pebbles, and gastropod grainstones. These features indicate the presence and passage of dunes that partially eroded underlying bedforms (Olariu et al., 2012). An upward transition from interbedded mudstone and fine-grained sandstone to alternating fine-grained and coarse-grained sandstone reflects an increase in shear stress associated with the passage of the dune complex. Features such as tidal bundling, clay drapes, sigmoidal cross-bedding, heterolithic cross-stratification, and herringbone cross-stratification provide evidence of a strong tidal influence on deposition (Dalrymple, 2010). A marine environment is supported by the presence of open marine taxa, including cephalopods and trilobites.

Mixed Carbonate–Siliciclastic Ramp Depositional System

The mixed carbonate–siliciclastic ramp depositional system preserves six environments represented by the offshore, deep subtidal, shallow subtidal, shoreface, sand flat, and transgressive lag facies associations (Table 2). Excluding the transgressive lag facies, these environments constitute much of the thickness of the eastern Ellis Bay Formation. While deep and shallow subtidal facies associations are well-developed and occur across the study area, shoreface and sandflat facies associations are largely restricted to updip exposures and tend to be much thinner than deeper-water facies associations (Fig. 3).

The offshore facies association (Mof) is restricted to downdip exposures of the eastern Ellis Bay Formation, including Rivière Natiscotec and Rivière aux Saumons. Offshore facies consist of thin- to medium-bedded mudstone interbedded with lenticular, graded wackestone and siltstone beds. An offshore setting is indicated by the thickness of the mudstone bodies and uncommon and distal storm beds (Aigner, 1982). Low-diversity fossil assemblages consisting of brachiopods and trilobites indicate a fully marine setting. Mof unconformably overlies members of the transgressive lag facies association and commonly grades up into deep subtidal facies (Mds) or abruptly passes into shallow subtidal facies (Mss).

The deep subtidal facies association (Mds) consists of very thin to thin tabular mixed carbonate–siliciclastic beds interbedded with mudstone. Evidence of storm activity, such as gradational beds with sharp, scoured bases; bioclastic lags; and concentrations of fossils differentiate the mudstone-rich (Mds1) and micritic (Mds2) deep subtidal facies from the offshore facies. Abundant rippled bedforms and hummocky cross-stratification in the rippled deep subtidal (Mds3) and hummocky deep subtidal (Mds4) facies associations indicate a strong storm and wave influence (Dott and Bourgeois, 1982); however, the tabular nature of bedding still suggests deposition within the deep subtidal setting (Droser and Bottjer, 1989; Pope and Read, 1998). Open marine fossil assemblages within these facies are commonly low diversity. Mds overlies members of the transgressive lag facies

association (Mtl) as well as the Mof in downdip exposures.

The shallow subtidal facies association (Mss) consists of highly bioturbated facies that are commonly nodular, a feature that is typical of Ordovician shallow subtidal settings (Droser and Bottjer, 1989; Holland and Patzkowsky, 1997; Pope and Read, 1998). Members of this facies association vary greatly in their lithology, which can include silty fossiliferous packstone (Mss1; amalgamated shallow subtidal), mudstone interbedded with sandy grainstone (Mss2; mudstone-rich shallow subtidal), pure lime mudstone (Mss3; micritic shallow subtidal), sandy peloidal grainstone (Mss4; laminated shallow subtidal), and lime mudstone with abundant siliciclastic pebbles (Mss5; pebble-rich shallow subtidal). While small unbioturbated windows preserve sedimentary structures such as hummocky cross-stratification and planar lamination in this facies association, most evidence of storm activity is almost completely destroyed by bioturbation. Shallow subtidal facies associations preserve diverse open-marine fossil assemblages with common disarticulation and fragmentation of skeletal elements. Members of this facies association commonly overlie Mds, with only a 10–50 cm gradational interval present at the transition between the deep and shallow subtidal facies associations.

The shoreface facies association (Msf) consists of erosionally based fine- to coarse-grained grainstone and sandstone that is either trough cross-bedded (Msf1), hummocky cross-stratified (Msf2), or can contain large rip-ups of the underlying facies (Msf3). Collectively, these features indicate a high shear-stress, shallow-water environment (Clifton, 2006). Fragmented open-marine fossils from each member of this facies association support the interpretation of a fully marine, shoreline proximal environment. All members of this facies association unconformably overlie Mds.

The sandflat facies association (Msd) is restricted to updip exposures, where it is composed of a mixture of calcareous sandstone and sandy peloidal grainstone, rarely interbedded with mudstone at the base of the facies association. Tidal influence is indicated by sigmoidal cross-bedding with tidal bundling, clay drapes,

TABLE 2. MIXED CARBONATE–SILICICLASTIC RAMP DEPOSITIONAL SYSTEM

Facies association and interpretation	Lithology and bedding	Sedimentary structures	Taphonomy	Contacts and context
Mof, offshore	Interbedded mudstone with very fine grainstone (calcisiltite), calcareous siltstone to very fine sandstone. Beds very thin, tabular. Mudstone in thin to medium beds.	Sharp-based beds overlain by skeletal lag.	Fossils, commonly whole and unabraded.	Occurs in Macairen and Natiscotecan sequences. Basal contact sharp, planed-off pyritic hardground. Grades upward into Mds.
Mds, deep subtidal				
Mds1, mudstone-rich deep subtidal	Interbedded mudstone with very fine packstone to grainstone (calcisiltite), commonly with silt to very fine siliciclastic sand. Beds very thin to thin, tabular, rarely subnodular. Mudstone in thin beds.	Sharp-based beds.	Fossils commonly whole or disarticulated, uncommonly fragmented.	Common in older sequences, gradational with underlying offshore facies (Mof). Overlain by shallow subtidal facies.
Mds2, micritic deep subtidal	Interbedded lime mudstone to grainstone with mudstone. Carbonate beds vary thin to medium at thickest, lenticular. Mudstone in laminated to thin beds.	Sharp-based beds with skeletal lags, normal grading. Beds rarely amalgamated. *Chondrites* abundant.	Fossils commonly whole, uncommonly pyritized. Moldic preservation common within Mauvaisen Sequence.	Basal contact, sharp flooding surface. Upper contact varies from sharp to gradational. Most widespread variant of Mds.
Mds3, rippled deep subtidal	Interbedded mudstone with calcareous very fine sandstone. Beds very thin to thin, tabular. Mudstone in laminated to medium beds.	Wave and interference ripples common, climbing ripples present. Rare amalgamated beds. *Cruziana* abundant.	Articulated crinoids common.	Only occurs in Natiscotecan Sequence at Rivière Schmitt. Base marked by sharp flooding surface. Facies capped by surface of forced regression.
Mds4, hummocky deep subtidal	Interbedded lime mudstone, very fine grainstone (calcisiltite), commonly silty, with mudstone. Beds vary from laminated to medium at thickest, subnodular to lenticular. Mudstone in laminated to medium beds.	Interference ripples and hummocky cross-stratification common in calcisiltite. In Mauvaisen Sequence, channels occur at top, with abundant rip-up clasts.	Fossils whole, unabraded.	Basal contact, sharp flooding surface. Beds thicken upward, showing trend of increasing storm proximality. Upper contact commonly abrupt transition to shallower facies.
Mss, shallow subtidal				
Mss1, amalgamated shallow subtidal	Interbedded silty fossiliferous packstone with mudstone. Beds vary from very thin to medium, rarely thick, tabular to nodular. Mudstone in laminated beds.	Beds nodular, bioturbation has obliterated primary sedimentary structures; small unbioturbated windows reveal hummocky cross-stratification. Amalgamation common.	Fossils fragmented.	Commonly overlies deep subtidal facies and capped by an abrupt flooding or combined surface.
Mss2, mudstone-rich shallow subtidal	Mudstone interbedded with calcareous sandstone and packstone to grainstone beds with siliciclastic sands. Beds very thin to thin, pseudonodular to nodular, often discontinuous. Mudstone in very thin to medium beds.	Beds nodular. Rare thin to medium sandstone beds with firmgrounds present at Anse Mauvaise. More highly bioturbated in the Macairen Sequence.	Fossils common, fragmented. Basal Prinstan contains abundant large calcifiers (e.g., tabulate corals, stromatoporoids, aulacerids). Gastropod *Hormotoma* abundant.	Present within Prinstan and Macairen sequences, commonly interbedded with or grading upward into sandflat facies (Msd).
Mss3, micritic shallow subtidal	Lime mudstone interbedded with mudstone. Beds very thin to thin, pseudonodular to nodular. Mudstone in laminated beds.	Beds nodular.	Lacks fossils.	Overlies deep subtidal facies in downdip localities where it is truncated by combined surface.
Mss4, laminated shallow subtidal	Peloidal grainstone to peloid-rich calcareous sandstone. Beds very thin to thin, tabular.	Laminated, but sedimentary structures often obliterated by intense bioturbation. Erosive base with angular rip-up clasts up to 30 cm in diameter.	Fossils uncommon, fragmented. Gastropod *Hormotoma* abundant.	Occurs at the top of the Mauvaisen Sequence across the study area.
Mss5, pebble-rich shallow subtidal	Light gray, very fine lime mudstone with layers of poorly sorted very coarse quartz and rare lithic (predominantly quartzite and chert) sand to pebbles. Beds thin to medium, nodular. Large (~50 cm) platy rip-up clasts at base of facies.	Bioturbation has obliterated primary sedimentary structures. Amalgamation and internal hardgrounds common.	Fossils commonly disarticulated.	Present at base of Mauvaisen Sequence in updip localities. Commonly capped by well-developed hardground.
Msf, shoreface				
Msf1, cross-bedded shoreface	Fine grainstone (common syntaxial cements) with quartz sand, lenses of mudstone. Mudstone in very thin lenses.	Trough cross-bedded in sets 30–50 cm thick. Well-rounded mudstone intraclasts 1–10 cm in diameter throughout.	Fossils commonly disarticulated but rarely fragmented.	Common in Natiscotecan Sequence, where it is found at the base and top of the sequence.
Msf2, hummocky shoreface	Silty grainstone. Thin to medium tabular beds of hummocky to swaley cross-stratification.	Large-scale hummocky to swaley cross-stratification.	Lacks fossils.	Present as thin intervals above deep subtidal facies, marking the tops of sequences.
Msf3, sandy shoreface	Fine to coarse sandy grainstone. Medium tabular beds. Contains large platy mudstone rip-ups from the underlying facies.	None.	Fossils rare, abraded, and disarticulated.	Present only at the top of the Natiscotecan Sequence at Rivière Schmitt, overlying Mds3.
Msd, sandflat	Interbedded peloidal grainstone to sandstone with mudstone. At Schmitt Creek, rare quartz pebbles. Sets thin to medium, mudstone interbeds laminated, present in troughs and channels. Facies coarsen upwards.	Sigmoidal cross-stratification in sets up to 10 cm thick. Tidal bundling and clay drapes. Wavy and lenticular bedding. Heterolithic cross-stratification. Channels present throughout sand bodies containing aulacerid accumulations.	Fossils tend to be disarticulated and abraded.	Commonly gradationally overlies Mss in updip localities.

(Continued)

TABLE 2. (*Continued*)

Facies association and interpretation	Lithology and bedding	Sedimentary structures	Taphonomy	Contacts and context
Mtl, transgressive lag Mtl1, transgressive lag	Bioclastic packstone to grainstone with quartz and rare to abundant lithic (predominantly quartzite and chert) sands to pebbles in lower (pre-Saumons) sequences. Beds very thin to thin, sometimes channelized. Common phosphate/pyrite-rimmed rip-up clasts.	None.	Fossils disarticulated and fragmented.	Found immediately above flooding surfaces at bases of sequences.
Mtl2, reworked sandstone	Calcareous very fine sandstone with mudstone, commonly removed by erosion. Beds tabular, very thin to thin. Mudstone in laminated beds.	Beds commonly amalgamated and capped by subtle bored hardgrounds.	Lacks fossils.	Present at base of Natiscotecan Sequence of Ruisseau Macaire and Rivière Schmitt, where it is capped by well-developed hardground.
Mtl3, condensed fossil bed	Crinoidal packstone to grainstone, interbedded with mudstone, commonly removed by erosion below overlying bed. Beds tabular, thin. Mudstone in laminated beds. Where it directly overlies sequence boundary, this facies contains quartz sands to pebbles.	Beds commonly amalgamated.	Fossils disarticulated and fragmented.	Present in lower part of Natiscotecan Sequence at Rivière aux Saumons, Ruisseau à la Batterie, and Ruisseau Macaire.

and flaser and wavy bedding, all of which suggest alternations in current strength and direction (Dalrymple, 2010). Msd contains shallow channels with current-aligned aulacerid stromatoporoids, stromatoporoids, and tabulate corals that also occur in situ within Msd, suggesting a fully marine setting. Where it does not overlie an unconformity, Msd can overlie Mss2.

The transgressive lag facies association (Mtl) is present at all exposures and consists of three distinct facies that are commonly capped by hardgrounds and overlain by Mof, Mds, or Mss. The transgressive lag facies (Mtl1) is composed of thin tabular to channelized bodies of bioclastic grainstone and packstone with quartz and rare lithic coarse sand to pebbles that form small pockets of conglomerate. Rounded and bored rip-up clasts derived from the underlying lithologies, rimmed by phosphate and pyrite, indicate a period of nondeposition and cementation of the seafloor (Sepkoski, 1982; Myrow et al., 2004). The reworked sandstone facies association (Mtl2) comprises tabular beds of calcareous, very fine-grained sandstone with rare mudstone interbeds. Beds are amalgamated and capped by subtle bored hardgrounds but do not preserve any identifiable sedimentary structures. The presence of abundant quartzose sand in the middle of an otherwise nearly clean carbonate unit is a common indicator of subaerial unconformities, which suggests that Mtl2 consists of reworked sands from an intervening period of subaerial weathering and erosion (Holland and Patzkowsky, 1996; Osleger and Montañez, 1996; García-Hidalgo et al., 2007; Wynn and Read, 2008; Read and Repetski, 2012). The presence of rare brachiopods indicates a marine setting. The condensed fossil-bed facies association (Mtl3) consists of tabular crinoidal grainstone and rare packstone beds. Condensation is indicated by the paucity of sedimentary grains other than crinoid ossicles that are highly resistant to degradation, as well as the abundance of authigenic pyrite (Scholle and Ulmer-Scholle, 2003). Grains other than crinoid ossicles are less common but include brachiopod valves, cephalopods, and, in some instances of this facies association, quartz grains of up to 1.5 cm in diameter.

Carbonate Ramp Depositional System

The carbonate ramp depositional system is composed of four facies associations within the study area. Three of these—the inner ramp, calcimicrobial patch reef, and siliciclastic shoal complex environments—are restricted to the Laframboise Member of the Ellis Bay Formation (Table 3; Fig. 3). The fourth, the deep subtidal facies (Mds4, Table 2), is present everywhere at the base of the Becscie Formation.

The inner ramp facies association (Cir) is composed of three facies. The transgressive inner ramp facies (Cir1) contains concentrically laminated oncoids of up to 3 cm in diameter, sand-sized peloids, and highly fragmented fossils, which suggests a high-shear stress inner ramp environment. Cross-bedding was previously reported for this facies (Desrochers et al., 2010). Cir1 fines upward and gradationally passes into Cir2, the peloidal inner-ramp facies, which preserves rare wave-ripple lamination. Cir2 commonly contains small calcimicrobial bioherms that range from small build-ups of tabulate corals to low-lying bioherms of ~1 m in height and diameter. At Ruisseau Macaire, Cir2 is overlain by the inner ramp sand-wave complex facies (Cir3). Small-scale trough cross-stratification with erosional set bases and opposing flow directions indicates oscillating current directions and a strong tidal influence, similar to conditions at other subtidal sand wave complexes (Blakey, 1984).

The final two facies associations are restricted to the area around Rivière aux Saumons and Rivière Natiscotec, where they occur in lateral association with one another. The patch reef complex facies association (Cpr) contains large, calcimicrobial patch reef complexes (up to 4–5 m thick and tens of meters in diameter) fringed by tabular bodies of crinoidal grainstone. Facies association Css is a starved siliciclastic shoal complex that is characterized by lenticular bodies of large-scale trough cross-bedding that in some places cut into underlying strata. Pebble lags consisting of fragments of Cir, Cpr, and oolitic grainstone, a lithology not observed in the study area, can be found as localized lags at the base of troughs. Similar starved siliciclastic shoals occur along carbonate shelves following the Last Glacial Maximum, where relict siliciclastic sands deposited during the previous lowstand systems tract were reworked by storm processes along the inner ramp (Testa and Bosence, 1998). Both Cpr and Css overlie Cir and are overlain by Mds4.

DEPOSITIONAL SEQUENCES

Along the eastern coast of Anticosti Island, the Ellis Bay Formation contains six depositional sequences, with the sixth sequence beginning at the base of the Laframboise Member and extending into the lowermost Fox Point Member of the Becscie Formation (Fig. 3). Each sequence is named for the exposure at which it is best developed, except for the Ballan Sequence, which is named for the soft-sediment deformation structure at the top of the sequence.

Sequence-stratigraphic nomenclature in this study follows the widely used four-systems

TABLE 3. CARBONATE RAMP DEPOSITIONAL SYSTEM

Facies association and interpretation	Lithology and bedding	Sedimentary structures	Taphonomy	Contacts and context
Cir, inner ramp				
Cir1, transgressive inner ramp	Oncoidal grainstone with peloids and skeletal fragments. Beds vary from thin to thick, tabular to lenticular in geometry. Abundant rip-up clasts at base and as cores of oncoids.	Overall fining upwards, with a decrease in size and abundance of oncoids.	Fossils fragmented, abraded, micritized, or covered by microbial layers.	Present at the base of the Saumons Sequence at all localities, but poorly developed at Ruisseau Macaire.
Cir2, peloidal inner ramp	Fine peloidal grainstone (nearly calcisiltite) with small calcimicrobe (~1 m in height and diameter) boundstones (bioherms). Beds very thin to thin, tabular.	Wave-ripple cross-lamination. Overall fining upwards.	Fossils fragmented, abraded.	Gradationally overlying Cir1.
Cir3, sand-wave complex	Coarse bioclastic grainstone, with variable amounts of quartz silt; syntaxial cement common. Beds irregular, very thin to thin, lenticular.	Small-scale trough cross-stratification with opposing foreset dip directions. Sets 3–10 cm thick.	Lacks fossils.	Only at Ruisseau Macaire, immediately overlying Cir2.
Cpr, patch reef complex	Large (~4–5 m in height, ~5–20 m in diameter) calcimicrobe boundstones (patch reefs) flanked by coarse grainstone with abundant crinoid ossicles. Beds very thin to thin, tabular.	None.	Fossils fragmented, abraded, often silicified or replaced by pyrite.	Directly overlying Cir1 in downdip settings, in lateral association with Cir3.
Css, starved siliciclastic shoal complex	Very fine to medium angular quartz sandstone. Beds laminated to medium, tabular. Contains pebble lags consisting of rounded fragments of C1, C2, and oolitic grainstone at the base of troughs.	Large-scale trough cross-stratification transitions laterally from horizontal beds, in sets 30–50 cm thick. Rip-up clasts of underlying or removed facies (e.g., ooid grainstone) at base of sets and in troughs.	Lacks fossils.	Commonly directly overlying Cir1 in downdip settings, in lateral association with Cir2.

tract model of Hunt and Tucker (1992), which includes the lowstand (LST), transgressive (TST), highstand (HST), and falling stage (FSST) systems tracts, which are also referred to as the depositional sequence (cf. Catuneanu et al., 2009). Zecchin and Catuneanu (2013) and Catuneanu et al. (2009) provide a detailed discussion of the four-systems tract model.

In this sequence-stratigraphic model, the sequence boundary is placed at the subaerial unconformity and correlative conformity that defines the base of the LST. In sequences where subaerial weathering and erosion has removed the underlying FSST, the subaerial unconformity can also lie at the upper bound of the HST or lower systems tracts. Following standard convention, sequence boundaries are named for the overlying sequence. In sequences where the LST is present, the maximum regressive surface (Helland-Hansen and Martinsen, 1996) separates progradational strata of the underlying LST from retrogradational strata of the overlying TST. Both the subaerial unconformity and maximum regressive surface can be eroded by waves during transgression, thus forming a composite surface with the transgressive ravinement surface. The maximum flooding surface, which separates the TST and HST, is commonly difficult to discern (cf. Zecchin and Catuneanu, 2013) because the turnaround from retrogradational to progradational stacking occurs within uniform distal facies. In these cases, the maximum flooding surface is approximated by where progradational patterns first become apparent above the flooding surface that marks the base of the deepest facies of each sequence. Where the FSST is present, the HST can be separated from the FSST by either the

basal surface of forced regression or a regressive surface of marine erosion. While the basal surface of forced regression marks the onset of forced regression, it can be difficult to identify from outcrop data alone (Bhattacharya, 2011). Although regressive surfaces of marine erosion are diachronous, they constrain the position of the FSST. Given the absence of seismic data that would demonstrate the seaward and downward shoreface trajectory diagnostic of the FSST, we place the boundary between the HST and FSST at the lowermost regressive surface of marine erosion (Fig. 3).

Prinstan Sequence

The basal surface of the Prinstan Sequence is exposed at Baie Prinsta and Anse Mauvaise, where it is characterized by a switch from the siliciclastic tidal depositional system to the mixed carbonate–siliciclastic ramp depositional system (Fig. 4). It coincides with the contact between the Vaureal and Ellis Bay formations sensu Copper et al. (2013). At Baie Prinsta, this surface is marked by decimeter-scale, stromatoporoid-encrusted mounds that protrude above erosive scours cut into the top of the underlying compound dune facies association (Tcd), whereas at Anse Mauvaise it is nearly planar and subtly scalloped (Figs. 4A and 4B). Sands from Tcd are reworked into the shallow subtidal facies (Mss2) in a thin interval above the contact, but well-cemented rip-up clasts of the underlying lithologies are absent. The basal surface of the Prinstan Sequence is therefore conservatively interpreted as a surface of maximum regression combined with a transgressive ravinement surface.

The exposed portion of the Prinstan Sequence consists predominantly of the HST of the sequence, which is characterized by the mixed carbonate–siliciclastic ramp depositional system. Where it is fully exposed, the Prinstan Sequences ranges from 5.9 m to 6.7 m thick. Above the flooding surface at Baie Prinsta and Anse Mauvaise, the sequence consists of a shallowing-upward package of the mudstone-rich, shallow subtidal facies (Mss2; Fig. 4B) conformably overlain by sandflat facies (Msd; Figs. 4C and 4D); the TST is largely absent or only present as a thin band at the base of the sequence. Poorly developed parasequences in Mss2 are capped by sandstone firmgrounds, which contrast with the highly bioturbated carbonate storm beds of Mss2. All other exposures consist of variants of deep subtidal facies. At Ruisseau Macaire, the mudstone-rich deep subtidal facies (Mds1) contains several omission surfaces with hummocky cross-stratification beds that may signify parasequence boundaries. West of Ruisseau Macaire, the proportion of mudstone relative to carbonate (predominantly lime mudstone) in deep subtidal facies progressively decreases downdip. This decreasing siliciclastic content is inferred to reflect an increase in the distance from a cratonic siliciclastic source that would have been in the present-day eastern part of the basin (Desrochers et al., 2010).

Macairen Sequence

The unconformity at the base of the Macairen Sequence is mantled by rounded quartz and rare lithic grains ranging from fine-grained sands to pebbles that are reworked into the transgressive lag facies (Mtl1; Fig. 5A). This siliciclastic
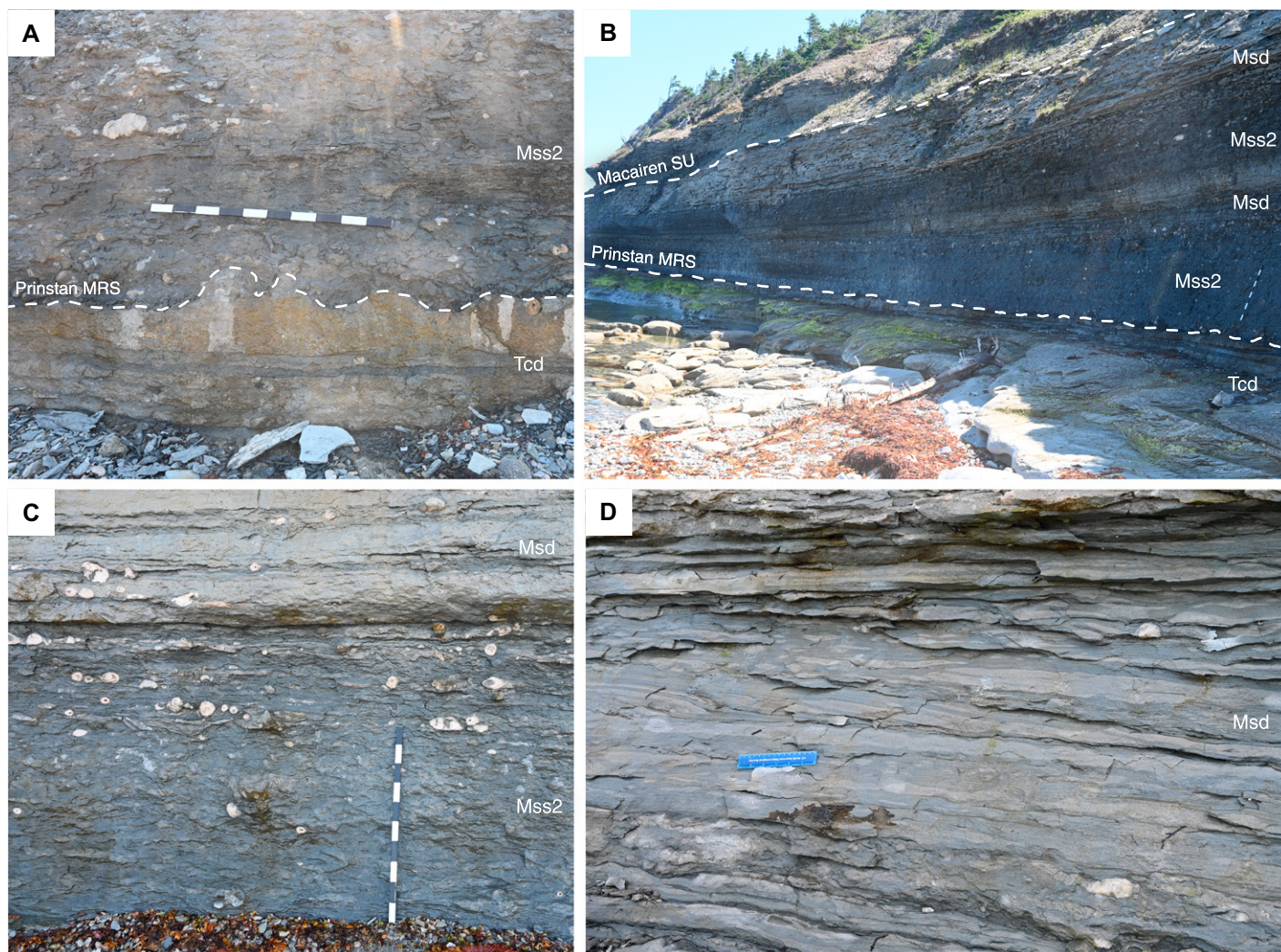
Figure 4. Facies and stratigraphic contacts of the Prinstan Sequence at Baie Prinsta, Québec, Canada. (A) Irregularly scalloped maximum regressive surface (MRS) at the base of the Prinstan Sequence is formed by differential erosion and encrustation/stabilization of the seafloor by stromatoporoids; the contact marks the transition from the tidal-influenced sands of the compound dune facies association (Tcd) to the nodular, mudstone-rich shallow subtidal facies (Mss2). (B) Exposure at the eastern end of Baie Prinsta capturing the transition from Mss2 to interbedded sandstone, grainstone, and mudstone of sandflat facies (Msd); the recessive slope atop Msd marks the deep subtidal facies at the base of the overlying Macairen Sequence, which is marked by a subaerial unconformity (SU). (C) Detail of Mss2 and overlying Msd showing dense accumulations of stomatoporoids and tabulate corals. (D) Wavy and lenticular bedding characteristic of Msd suggests tidal influence.

lag is best developed at Ruisseau Macaire and Ruisseau à la Batterie, where dense accumulations of siliciclastic sand and gravel in Mtl1 form patches of calcareous conglomerate with irregular phosphate- and pyrite-rimmed rip-up clasts. Similar surfaces mantled by siliciclastic sands and pebbles in carbonate-dominated intervals are important indicators of subaerial weathering and erosion, representing a significant fall in base level that enabled the delivery of relatively coarse siliciclastic sediment into a generally carbonate-dominated system (Bambach, 1988; Haynes, 1992; Budd et al., 2002; Saylor, 2003). In updip exposures, the uncon-

formity is a scoured and burrowed surface filled in by Mtl1 and marked by a black and purple stain at the top of the underlying sandflat facies (Fig. 5B). In downdip exposures, the unconformity is marked by a thin, blackened, phosphatized hardground with irregular cavities and pockets, rimmed by diagenetic halos and filled by Mtl1. These features support the interpretation that the base of the Macairen Sequence is a combined subaerial unconformity and transgressive ravinement surface.

At Rivière Schmitt, the basal unconformity of the Macairen Sequence is marked by an incised valley at least 15 m deep; comparison

to updip exposures suggests that this surface truncates the entirety of the Prinstan Sequence at Rivière Schmitt. The valley fill consists of a succession of sandflat and tidal facies (Figs. 5C and 5D) that abruptly overlies underlying deep subtidal facies (Mds). Tidal currents during transgression likely reworked any fluvial facies originally deposited at the base of the valley (Smith and Read, 2000). Facies of this valley preserve an aggradational stacking pattern that is terminated by a flooding surface mantled by a dense lag of siliciclastic sand and pebbles, as well as rounded rip-up clasts, which mark a maximum regressive surface
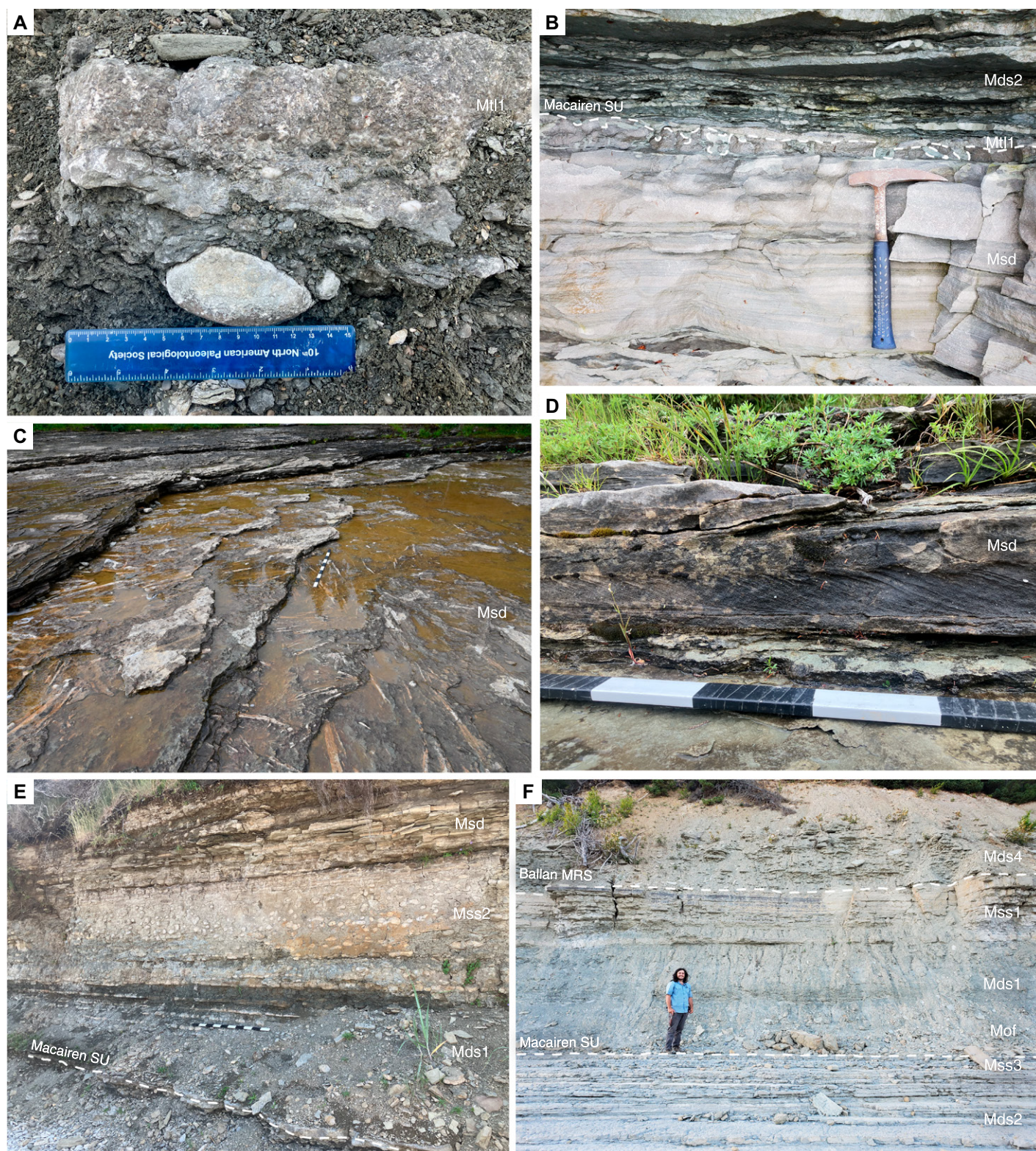
reworked by transgressive ravinement; a similar succession has been observed 2 km to the west at Rivière Petite Meule. The valley fill is therefore considered to be part of the LST and records some of the earliest deposition of the Macairen Sequence (Driese et al., 1994; Grélaud et al., 2006).

The Macairen Sequence is composed of the mixed carbonate–siliciclastic ramp depositional system. Above the maximum regressive surface, the sequence ranges from 2.5 m to 6.0 m in thickness. Above the lag facies (Mtl) mantling the transgressive ravinement surface, facies contacts within this sequence are gradational and record a progradational stacking of facies,

Geological Society of America Bulletin

Figure 5. Photos of the Macairen Sequence. (A) In situ portion of the transgressive grainstone lag facies (Mtl1) at the base of the sequence at Baie Prinsta containing well-rounded quartz pebbles. (B) Subaerial unconformity (SU) of the Macairen Sequence at Anse Mauvaise; where it is not removed by the transgressive surface, the upper several centimeters of the top of the Prinstan Sequence are darkly stained and marked by irregular pockets and cavities interpreted as microkarst. This surface is overlain by micritic deep subtidal facies (Mds2) with abundant *Hindella*, a common component of transgressive facies. The hammer used for scale is roughly 30 cm long. (C) Dense accumulations of aulacerids in thin, channelized beds within sandflat facies (Msd) at Rivière Schmitt. (D) Detail of Msd from the lowstand systems tract (LST) at Rivière Schmitt showing sigmoidal cross-bedding and tidal bundling of fine-grained and coarse-grained sandstone layers. (E) Nearly complete succession of the Macairen Sequence at Baie Prinsta, with transgressive lag facies (Mtl1) (top of shelf at base of exposure) overlain by the micritic deep subtidal facies (Mds) that subsequently grade up into nodular, mudstone-rich shallow subtidal facies (Mss2). At the top of this photo, Mss2 passes upward into sandflat facies (Msd). (F) Exposure of at Rivière aux Saumons capturing the gradational contacts within the sequence. Offshore facies (Mof) pass upward into deep subtidal facies (Mds1), followed by a gradual transition to shallow subtidal grainstone of facies Mss1, which is capped by the Ballan Sequence maximum regressive surface (MRS).

which suggests that the preserved portion of the Macairen Sequence largely records deposition during the HST (Figs. 5E and 5F). The distribution of facies within the sequence reflects the gentle southwestward slope of the ramp. Offshore facies (Mof), present at the base of the sequence in downdip exposures, do not extend eastward beyond Ruisseau à la Batterie, while sandflat facies (Msd), which cap the sequence in updip exposures, do not extend westward of Rivière Schmitt.

Ballan Sequence

The base of the Ballan Sequence is a maximum regressive surface that is marked by an abrupt transition from shallow subtidal and sandflat facies to deep subtidal facies across the study area. There is no evidence of subaerial weathering or erosion at the base of the sequence, making it difficult to definitively place the Ballan sequence boundary (Fig. 3). The maximum regressive surface is immediately overlain by a thin interval of Mtl1, which is notable for the abundance of the gastropod *Hormotoma gigantea* and the presence of large tabulate corals of up to several decimeters in diameter. It is marked by the peak of the lower Hirnantian isotope carbon excursion (HICE; sensu Mauviel and Desrochers, 2016) at many exposures, which provides an additional means for correlation across the eastern Ellis Bay Formation (Fig. 6).

At every exposure, the Ballan Sequence is dominated by deep subtidal facies (Mds4), indicating overstep and maximum flooding of the ramp (Figs. 7A–7C); the sequence ranges from 2.5 m to 4.9 m in thickness. Mds4 is notable for its strong evidence of storm influence that becomes better developed from the base to the top of the facies. In many outcrops, this trend is the only evidence of shallowing. Exceptions are a thin interval of lower shoreface (Msf2), and a thin interval of shallow subtidal facies (Mss3) abruptly overlying Mds4 at Anse Mauvaise and Rivière Natiscotec,

respectively. These contacts may represent a regressive surface of marine erosion that marks the base of the FSST at each locality. A planed-off saucer structure (sensu McLaughlin and Brett, 2004) marks the top of the Ballan Sequence along the outcrop belt from Anse Mauvaise to Ruisseau Macaire (Figs. 7C and 7D). Zones of intense deformation 0.2–2.5 m thick can be traced along coastal outcrops for tens of meters before pinching out, only to reappear at the same horizon farther along the exposure a kilometer or more away. Given the rarity of soft sediment deformation structures in the succession, the distinctive Ballan saucer structure is attributed to a single event, perhaps due to a combination of seismic (possibly the activation of subsurface faults; Bordet et al., 2010) and eustatic (forced regression and slope instability; McLaughlin and Brett, 2004) processes.

Natiscotecan Sequence

The unconformity at the base of the Natiscotecan Sequence is a sharp erosional surface with centimeters to decimeters of relief; it is mantled by a lag of phosphate and pyrite-rimmed, bored rip-up clasts and rounded quartz pebbles that are reworked into the facies of the transgressive lag facies association (Fig. 8). At Baie Prinsta, Mtl1 is present only where the unconformity truncates the axes of the Ballan saucer structure, but the rip-up clast and quartz pebble lag can be traced continuously above intervening stretches of undeformed strata (Figs. 7D and 7E). In downdip exposures, the erosional nature of the contact is visible only in hand samples and thin sections, where the surface is sharp, rimmed by a diagenetic halo, and abruptly overlain by Mtl1 or Mtl3, both of which contain common quartz sand and pebbles (Figs. 8A and 8B). These features suggest that the base of the Natiscotecan Sequence is a subaerial unconformity combined with a transgressive ravinement surface (Bambach, 1988; Haynes, 1992; Hillgaertner, 1998; Budd et al., 2002; Saylor, 2003).

The Natiscotecan Sequence ranges from 3.3 m to 8.3 m thick and shows a marked increase in thickness moving westward and downdip. Transgressive lag facies at the base of the Natiscotecan Sequence are well-developed between Rivière Schmitt (Mtl2) and Ruisseau à la Batterie (Mtl1 and Mtl3), where a series of condensed facies record the earliest stages of relative sea-level rise during the TST. Downdip, these facies pinch out to a thin interval of the condensed fossil-bed facies (Mtl3) that is capped by a well-developed phosphatic hardground, with borings and meter-sized, planed-off cephalopods, that marks a major flooding surface (Fig. 8C). Above this surface, downdip exposures record a package of offshore facies (Mof) that are abruptly overlain by a thick interval of shallow subtidal sediments (Mss1; Fig. 8D); this non-Waltherian facies contact defines a regressive surface of marine erosion marking the base of the falling stage systems tract (Zecchin and Catuneanu, 2013). Farther updip, exposures are dominated by deep subtidal facies that record a subtle upward increase in siliciclastic grain size and bed thickness that is abruptly overlain by shoreface deposits (Figs. 8E, 8F, and 9A–9C). This abrupt juxtaposition of shoreface siliciclastic facies atop deep subtidal carbonate facies is a common expression of forced regression in mixed carbonate–siliciclastic settings (Zecchin and Catuneanu, 2017).

Mauvaisen Sequence

The basal unconformity of the Mauvaisen Sequence is traceable from Anse Mauvaise to Rivière Natiscotec. In updip exposures, it is marked by a subtle erosional surface with sharply defined pits and pockets cut into underlying shoreface facies (Fig. 9B); vadose silts, calcite-filled vugs, and meteoric cements were reported from immediately below the unconformity at Anse Mauvaise (Desrochers et al., 2010). Above this surface, a lag consisting of rounded quartz and rare lithic grains, ranging from medium-grained sands to pebbles, and
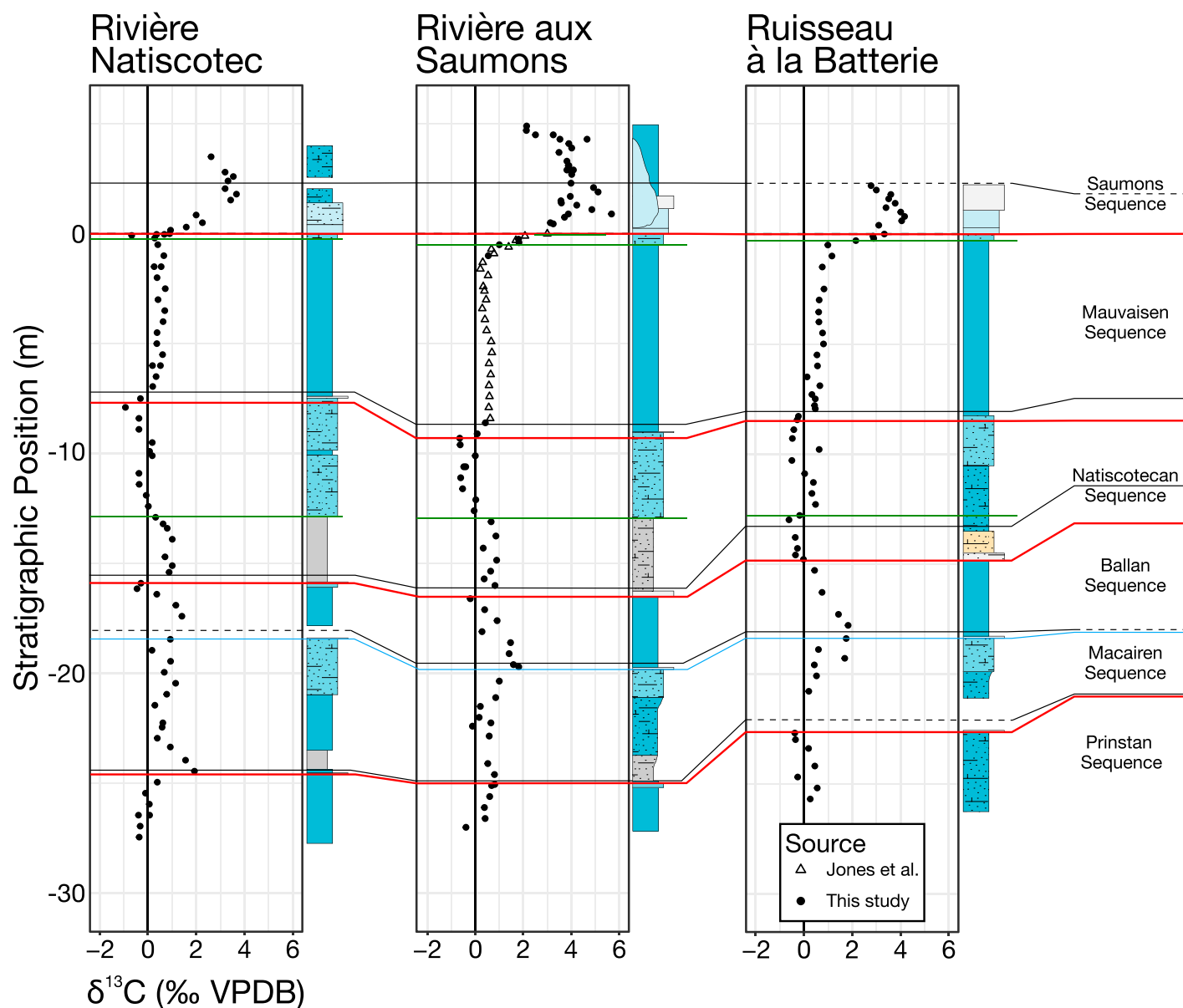
Figure 6. Carbon isotopic profiles for each locality plotted within the context of the sequence stratigraphic framework of the Ellis Bay Formation, using the base of the Saumons Sequence as a datum. This surface corresponds to the base of the Upper Hirnantian isotope carbon excursion (HICE) sensu Mauviel and Desrochers (2016). A small positive carbon isotope excursion at the contact of the Macairen and Ballan sequences marks the lower HICE of Mauviel and Desrochers (2016). See Figure 3 for key to facies and surfaces. VPDB—Vienna Peedee belemnite.

decimeter-scale platy rip-up clasts of the under-lying lithologies are reworked into the lower-most pebble-rich shallow subtidal facies (Mss5; Fig. 9C). The presence of hardgrounds within Mss5 indicates periodic sediment starvation and condensation in a subtidal setting (Gómez and Fernández-López, 1994; Föllmi, 2016). Mss5 is overlain by deep subtidal facies (Mds).

In downdip exposures west of Ruisseau Macaire, the basal unconformity of the Mau-vaisen Sequence is placed at an abrupt change from nodular to tabular bedding within Mss1,

which coincides with a marked decrease in bed thickness. At Ruisseau à la Batterie, Rivière aux Saumons, and Rivière Natiscotec, depleted carbon isotopic values occur below this change in bedding (Fig. 6). Comparison to isotopic data from the Mss1 facies of the Macairen Sequence suggests that this deple-tion cannot be explained as a facies-specific effect; furthermore, isotopic data from more distal exposures of the western Ellis Bay For-mation do not record this depletion (Mauviel and Desrochers, 2016). Instead, this isoto-

pic depletion is interpreted to reflect mete-oric diagenesis during a period of subaerial weathering and erosion (Allan and Matthews, 1982; Driese et al., 1994; Railsback et al., 2012). The base of the Mauvaisen Sequence is therefore interpreted as a combined sub-aerial unconformity and transgressive ravine-ment surface.

The Mauvaisen Sequence gradually increases in thickness from Anse Mauvaise to Rivière aux Saumons, increasing from 5.9 m to 9.2 m thick. Lowermost strata of the Mauvaisen Sequence
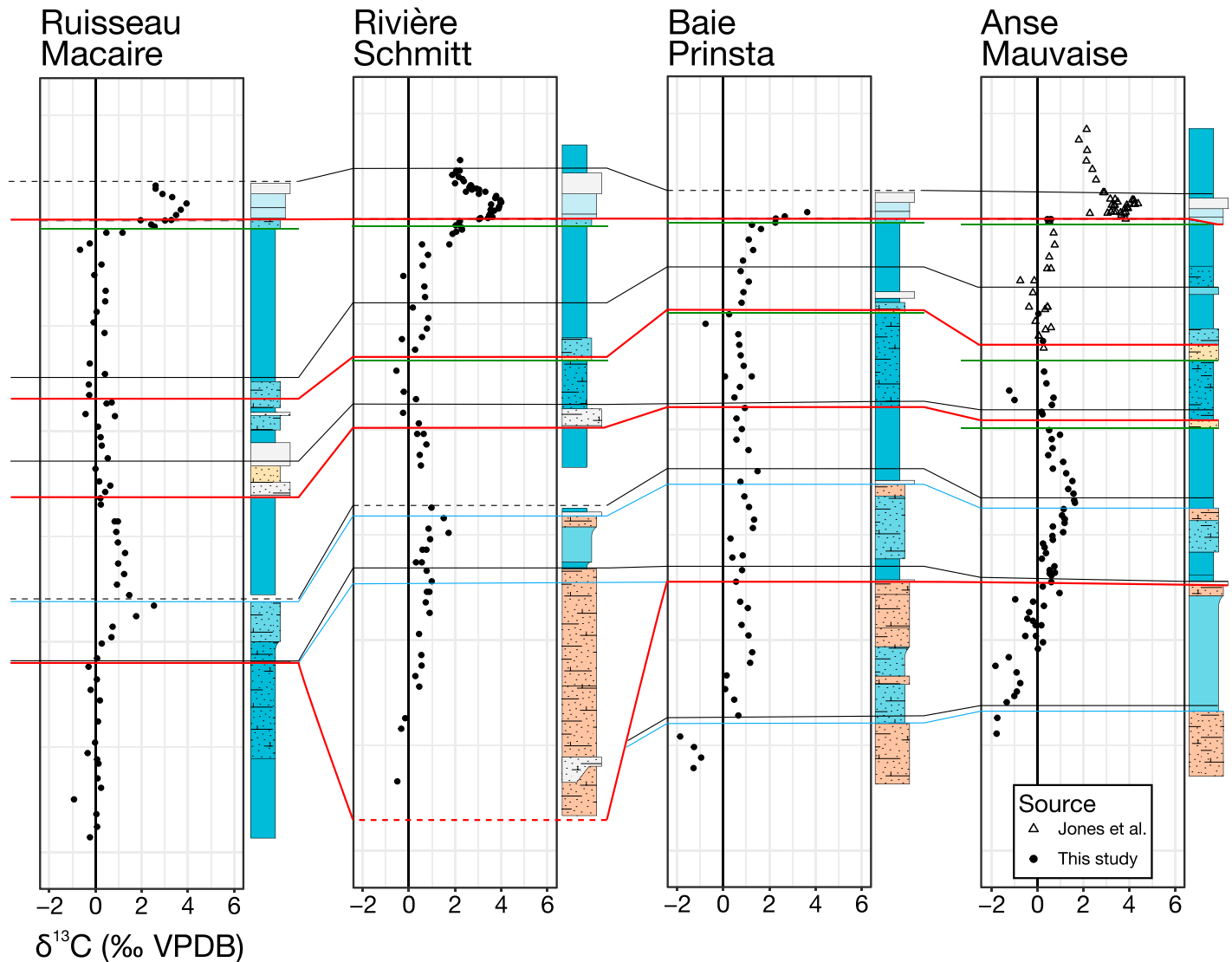
Figure 6. (*Continued*)

are characterized by stratigraphic condensation, including multigenerational flat pebble conglomerates and well-developed hardgrounds that mark the base of the micritic deep subtidal facies (Mds2; Fig. 9D). However, Mds2 constitutes nearly the entire sequence in downdip settings, obscuring the boundary between the TST and HST (Fig. 9E). Updip at Anse Mauvaise, the TST is defined by a single parasequence that records the alternation between shallow and deep subtidal facies (Fig. 9A). At the top of this parasequence, a well-developed hardground marks the base of a thick interval of deep subtidal facies, demarcating the lower bound of the HST. While hardgrounds are also present at Baie Prinsta, Rivière Schmitt, and Ruisseau Macaire, these surfaces are not correlative. An interval of convolute bedding (sensu McLaughlin and Brett, 2004), ~1.5 m below the

most prominent hardground at Anse Mauvaise (Fig. 9F), can be traced westward along the coastline as it transitions to a saucer structure located above another prominent hardground present at the base of the sequence both at Baie Prinsta (Fig. 9G) and Rivière Schmitt. This suggests that the hardground at Anse Mauvaise (marking the base of the HST) cannot be correlated with hardgrounds farther downdip. The maximum flooding surface at Baie Prinsta and Rivière Schmitt is therefore tentatively placed at an interval of thick mudstone and a thin, blackened, phosphatized hardground within Mds2, respectively. Farther downdip, the maximum flooding surface is placed in the lower portion of Mds2, which characterizes nearly the entire sequence at these localities.

Above the maximum flooding surface, subtle evidence of shallowing is indicated by an

increase in the number of packstone and grainstone storm beds within Mds2. The facies is erosively overlain by the laminated shallow subtidal facies (Mss4), which contains abundant large, angular rip-ups of Mds2 at its base (Figs. 10A and 10B). Given the lack of evidence for significant shallowing immediately prior to this transition, the abrupt, erosive transition from a deep subtidal to a shallow subtidal/inner ramp environment is interpreted as a regressive surface of marine erosion that marks the base of the FSST of the sequence at each locality.

Saumons Sequence

The base of the Saumons Sequence is a well-defined subaerial unconformity that is traceable across the eastern Ellis Bay Formation; this surface coincides with the base of the Lafram-
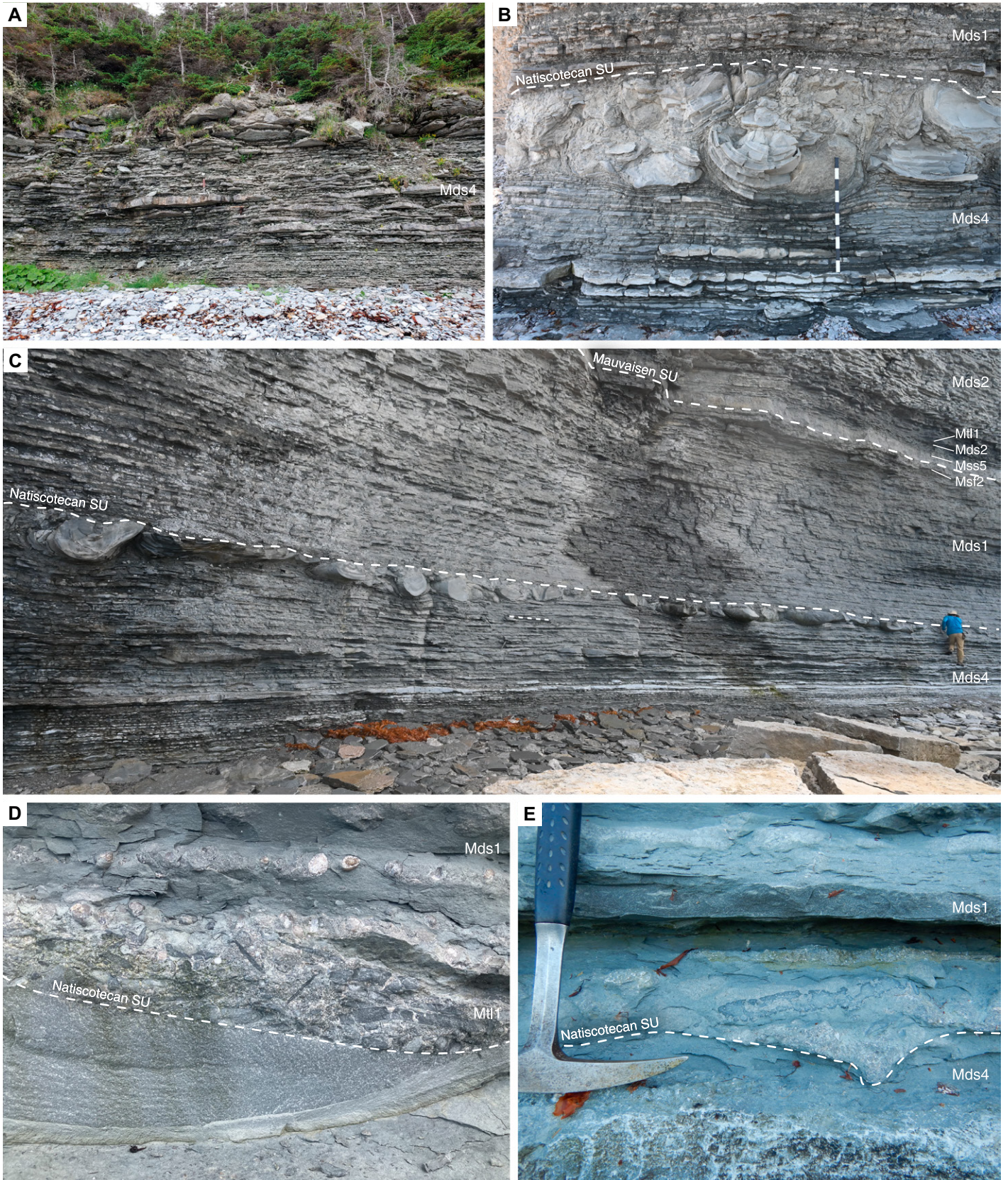
Figure 7. Photos of the Ballan Sequence. (A) Interbedded lime mudstone and calcisiltite of the deep subtidal facies Mds4 at Anse Mauvaise; the lower contact of the saucer structure at the top of the Ballan Sequence is exposed just below the tree line. (B) East of part A, the Ballan soft-sediment deformation structure is well exposed. Note that the top of the saucer structure has been planed off, marking the subaerial unconformity (SU) of the Natiscotecan Sequence. (C) Exposure of the Ballan saucer structure at Baie Prinsta, where its planed-off upper contact coincides with the sequence boundary between the Ballan and Natiscotecan sequences. (D) Detail of the saucer structure from part C, showing how the axes of the loads have been irregularly eroded, with lows filled by a transgressive lag (transgressive lag facies association; Mtl1) consisting of phosphate and pyrite-rimmed rip-up clasts and quartz pebbles in grainstone. (E) Where the saucer structure is not present at the top of the Ballan Sequence at Baie Prinsta, large, extensively bored, phosphate and pyrite-rimmed rip-up clasts and sparse quartz pebbles mantle the subaerial unconformity that separates the Ballan and Natiscotecan sequences. Hammer is 30 cm long.

◄————————————————————————————————

boise Member, sensu Long and Copper (1987a) and Copper et al. (2013). Evidence of subaerial weathering and erosion is best expressed in updip exposures, where the surface is sharply defined and varies in expression from flat, with irregular cavities cut below the surface, to undulatory, ranging from centimeter-scale pitting to significant relief of up to 30 cm (Figs. 10C–10F). In some places, such as at Anse Mauvaise and Baie Prinsta, inner ramp facies at the top of the Mauvaisen Sequence have been completely eroded, and large platy rip-up clasts (up to ∼50 cm in diameter) of underlying lithologies mantle the unconformity. Moving westward, evidence of subaerial weathering and erosion becomes more subtle and is expressed as pitting, small, irregular cavities, and a sharp, eroded surface (Fig. 10F). These features suggest that the base of the Saumons Sequence is a combined subaerial unconformity and transgressive ravinement surface (Zecchin and Catuneanu, 2013).

The TST of the Saumons Sequence is characterized by the carbonate ramp depositional system. At nearly every exposure, the unconformity is overlain by a well-developed transgressive inner ramp facies (Cir1); the one exception is Ruisseau Macaire, where only a thin layer of oncoids mantles the unconformity. Cir1 fines upward and gradationally passes into the peloidal inner ramp facies (Cir2), which is either overlain by the sand-wave complex facies (Cir3), the patch reef complex facies (Cpr; Fig. 10G), or the starved siliciclastic shoal complex facies (Css; Fig. 10H). Both Cpr and Css are restricted to downdip exposures, where they can be laterally interspersed with one another. In some cases, rip-up clasts of ooid grainstone, a facies that is not present in situ at any exposure, are reworked in Css.

The shallow-water facies of the carbonate ramp depositional system are capped by a phosphatic hardground across the eastern Ellis Bay Formation that drapes the bioherms protruding above the surface. Reddish staining of this surface at Rivière aux Saumons indicates local enrichments of pyrite that were subsequently oxidized. Previous studies interpreted

this sharply defined surface as a subaerial unconformity based on its paleorelief (in western outcrops), small-scale ridges and grooves, and the rounded pebble intraclast lags that mantle this surface (Desrochers et al., 2010); however, these features also could have formed in an entirely marine setting through transgressive ravinement. In the study area, the surface displays no unequivocal evidence indicative of subaerial weathering and erosion such as paleokarst, incision, a light carbon isotopic spike, quartz pebble lags, or meteoric cements that mark subaerial unconformities in other sequences of the Ellis Bay Formation (Hillgaertner, 1998; Pope and Read, 1998; Brenchley et al., 2006; Grélaud et al., 2006; Railsback et al., 2012). Given the lack of definitive evidence to support a subaerial origin for the formation of this surface, the upper contact of the carbonate ramp depositional system in the study area is best described as a major flooding surface associated with sediment starvation and potential shutdown of the carbonate factory. It is overlain by a coarse, megarippled transgressive lag (Mtl1) that is commonly blackened, with phosphate-replaced grains, which indicate a prolonged period of condensation associated with flooding of the ramp (Föllmi, 2016). At all exposures, Mtl1 is followed by Mds4, which onlaps the bioherms that protrude above the flooding surface. Where the HST of the Saumons Sequence is well-exposed, carbonate beds of Mds4 display a thickening-upward trend, which broadly suggests progradation. The upper contact of the Saumons Sequence is not exposed at any locality.

DISCUSSION

Stratigraphic Architecture of the Ellis Bay and Lowermost Becscie Formations

Depositional sequences of the Ellis Bay and lowermost Becscie formations are broadly similar in their architecture, being dominated by progradational and forced-regressive stacking patterns (Fig. 3). A typical depositional sequence begins with a combined subaerial unconformity and transgressive ravinement surface that is

almost planar, reflecting erosional truncation of the subaerial unconformity (Zecchin and Catuneanu, 2013). For most depositional sequences, the LST is absent or, in the rare case of a minor relative sea-level fall, poorly developed and indistinguishable from the underlying HST, such as across the Macairen–Ballan contact. This is expected given the distance of the study area from the shelf break (Catuneanu, 2006).

The exception to this pattern is the valley fill within the Macairen Sequence at Rivière Schmitt, which is filled by a thick succession of tidally influenced facies that suggests a fall in relative sea level of at least 15 m. Exposures examined in this study most likely do not capture the full width or the maximum depth of erosion of the incised valley at the base of the Macairen Sequence. The predominantly siliciclastic facies of the uppermost Vaureal Formation and Prinstan Sequences in updip settings, as well as the conspicuous presence of tidal processes, markedly contrast with the storm-dominated, carbonate-dominated facies that characterize facies at localities downdip from Rivière Schmitt. Studies of other icehouse carbonate ramps reported that tidally influenced siliciclastics are common features of valley fills (Smith and Read, 2000), which suggests that the valley at the base of the Macairen Sequence may be one part of a larger incised valley system. Further data from the uppermost Vaureal Formation along the eastern coast of Anticosti Island will be critical for understanding the full extent of this incised valley system.

In most depositional sequences of the study area, transgressive ravinement surfaces are overlain by the transgressive lag facies association (Mtl) that often constitutes most of the TST. A rapid rise in relative sea level, coupled with the low gradient of the ancient ramp, would have outpaced the rate of carbonate production and trapped siliciclastic grains in nearshore settings, producing a thin TST (Cattaneo and Steel, 2003; Zecchin, 2007; Zecchin and Catuneanu, 2017). In some sequences, the lag is overlain by a series of relatively thin facies that reflect conditions of sediment starvation and/or condensation during the TST. Rare, nearly pure siliciclastic facies in TSTs (e.g., the Natiscotecan Sequence) would
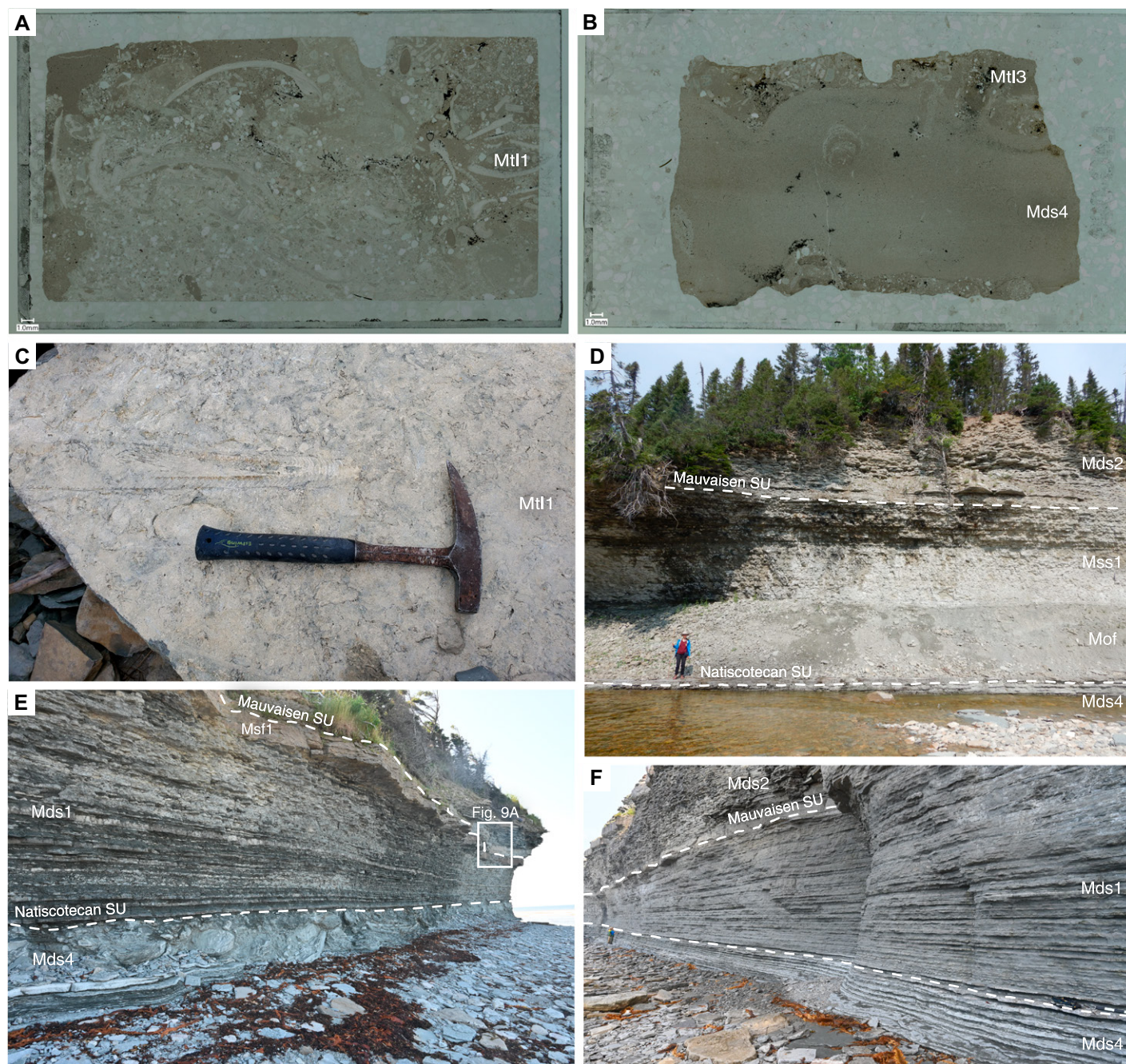
Figure 8. Photographs of the Natiscotecan Sequence. (A) Thin section of the basal transgressive grainstone facies (Mtl1) at the base of the sequence at Rivière Natiscotec. Quartz pebbles and sand reworked into the transgressive lag contrast with the fine-grained facies below and above Mtl1. (B) Thin section capturing the Ballan/Natiscotecan contact (sharp surface at top of thin section) at Rivière aux Saumons. Here, the condensed fossil bed facies (Mtl3) has a sharp, irregular contact with the underlying deep subtidal facies (Mds4) of the Ballan Sequence, but also fills in burrows below the contact. (C) At Rivière Natiscotec, a phosphatic hardground with large, planed-off, meter-sized orthocone nautiloids marks the top of Mtl1. Hammer is 30 cm long. (D) Complete exposure of the Natiscotecan Sequence at Rivière Natiscotec, with the Natiscotecan subaerial unconformity (SU) right above river level. The bench above river level is the hardground in part C, above which offshore facies (Mof) are abruptly overlain by thick-bedded grainstone of the amalgamated shallow subtidal facies association (Mss1). (E and F) Complete exposure of the Natiscotecan Sequence at Anse Mauvaise and Baie Prinsta, respectively. At both exposures, deep subtidal facies (Mds1, Mds2, and Mds4) are abruptly overlain by trough cross-stratified grainstone and sandstone of the shoreface facies Msf1. For detailed views of the Natiscotecan/Mauvaisen contact, see Figure 9.
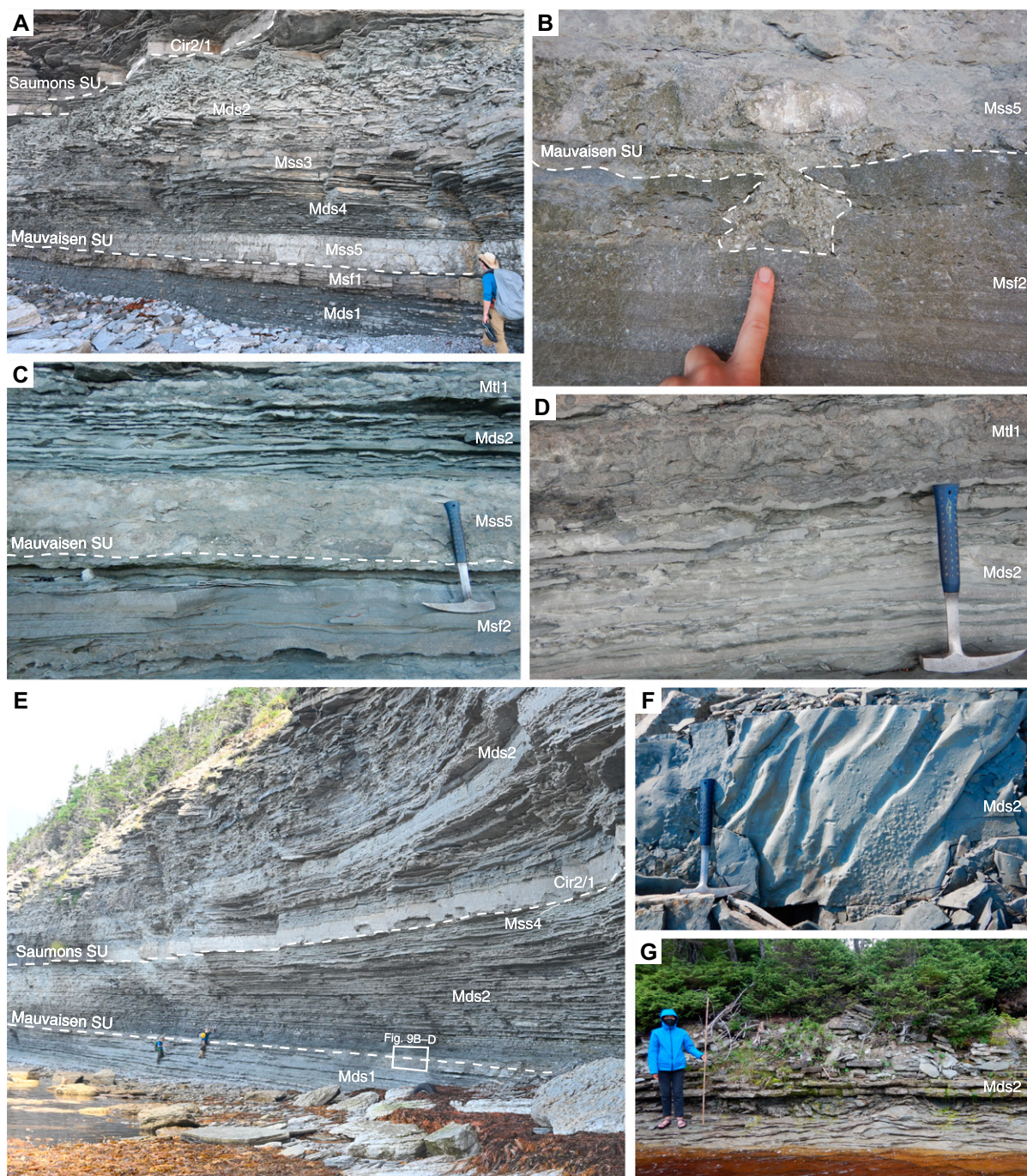
Figure 9. Photographs of the Mauvaisen Sequence. (A) Exposure of the Mauvaisen Sequence at Anse Mauvaise, where the contact between the shoreface facies Msf1 (red) and nodular pebble-rich shallow subtidal facies Mss5 (white) marks the subaerial unconformity (SU) at the base of the Mauvaisen Sequence; it is overlain by a succession of deep Mds and shallow Mss subtidal facies (Mds2, Mds4, Mss3, and Mss5). (B and C) Details of the Mauvaisen subaerial unconformity at Baie Prinsta showing microkarst pockets filled by pebble lags at the base of the overlying Mss5 facies and large, irregular rip-up clasts of the underlying Msf1 reworked into the lag at the base of Mss5. (D) Condensed transgressive lag facies Mtl1 just above the base of the sequence at Baie Prinsta with multiple generations of phosphate and pyrite-rimmed rip-up clasts beneath a well-developed hardground surface, suggesting multiple episodes of starvation and/or condensation. (E) Full exposure of the sequence at Baie Prinsta, dominated by lenticular lime mudstone of the micritic deep subtidal facies Mds2. The top of the sequence is marked by a pronounced grainstone bed (see Fig. 10). (F) Bedding-plane view of convolute bedding above the Mauvaisen subaerial unconformity, but below the maximum flooding surface of the sequence, at Anse Mauvaise showing broad antiforms and synforms along the deformed seafloor. (G) Saucer structure north of the bridge crossing Rivière Prinsta at Baie Prinsta, located above the maximum flooding surface of the Mauvaisen Sequence.

presumably have been sourced from reworked sediments that were deposited on the ramp during the FSST and LST of the previous sequence (Khetani and Read, 2002; Wynn and Read, 2008; Read and Repetski, 2012; Testa and Bosence, 1998).

In nearly all sequences, shallow-water facies of the TST are abruptly overlain by deeper-water carbonates and mudstones, reflecting a rapid rise in relative sea level. Progradational patterns in the HST are indicated by shallowing-upward facies stacking patterns or, where the HST consists of a single facies (e.g., in the Ballan, Mauvaisen, and Saumons sequences), increases in the frequency, thickness, and proximality of storm beds. Siliciclastic and shallow-water carbonate facies abruptly overlying finer-grained offshore and deep subtidal facies reflect the down-stepping of the shoreline during the FSST (Zecchin and Catuneanu, 2017). The regressive surface of marine erosion at the base of these erosively based deposits is commonly mantled by large rip-up clasts of the underlying lithologies, which indicates a prolonged period of sediment bypass and seafloor cementation during forced regression (Pattison, 1995; see Zecchin and Catuneanu, 2017). In some cases, and rather atypically, FSSTs comprise the thickest part of the depositional sequences in the study area (e.g., the Natiscotecan Sequence).

Evidence of Subaerial Weathering and Erosion in the Ellis Bay Formation

Subaerial unconformities in the eastern Ellis Bay Formation are traceable across the study area, enabling the recognition of six depositional sequences within the Ellis Bay and lowermost Becscie formations (Fig. 3). These unconformities are commonly combined with the transgressive ravinement surface, which may remove or rework evidence of subaerial weathering and erosion (Zecchin and Catuneanu, 2013; Figs. 5B, 7D, 8A, 9B, and 10B–10F). Each of these unconformities represents a substantial gap in the stratigraphic record and reflects a combination of nondeposition and erosion

associated with relative sea-level fall and transgressive ravinement. Notably, evidence of subaerial weathering and erosion at each of these surfaces becomes increasingly subtle westward and downdip due to an inferred shorter duration of subaerial exposure and an increased period of bypass and nondeposition during transgression resulting from siliciclastic sequestration in nearshore areas and the reestablishment of the carbonate factory (Figs. 10D–10F). Siliciclastic grains reworked into the transgressive lag and lower part of the TST commonly mark unconformities in downdip exposures that would otherwise be cryptic. These lags vary from lenses of pebble conglomerates to horizons of sparse quartz pebbles, but they can all be traced along unconformities to updip exposures. The broad distribution of these thin horizons of siliciclastic sand and gravel over an area of the ramp previously dominated by carbonate production indicates a dramatic shift in sedimentation patterns within the predominantly fine-grained mixed carbonate–siliciclastic ramp depositional system, which require a marked increase in the volume and rate of transport of siliciclastic sediment to the inner and mid-ramp. Long-term changes in weathering or tectonic uplift that may modify siliciclastic source areas would be unlikely to produce such intermittent and brief pulses of siliciclastic sand and gravel to the ramp (e.g., Pope and Read, 1998; Saylor, 2003). These are instead attributed to high-frequency glacioeustatic fluctuations, which would have repeatedly flooded and drained epicontinental seas during the Hirnantian Stage, generating intermittent increases in both the source area and rate of transport of siliciclastic grains to the ramp (Read, 1998; Khetani and Read, 2002; García-Hidalgo et al., 2007). The incised valley at the base of the Macairen Sequence suggests that relative sea-level changes in the Anticosti Basin were sufficient for rivers to incise deep valleys and transport siliciclastic material to settings that were previously in mid-ramp positions (Driese et al., 1994; Grélaud et al., 2006). These siliciclastics would have been subsequently reworked by waves during transgression and incorporated

into the TST as lags and reworked siliciclastic facies (Haynes, 1992; Saylor, 2003; Wynn and Read, 2008; Read and Repetski, 2012).

At the outcrop scale, geometries of subaerial unconformities tend to be flat to broadly undulatory but can locally have several decimeters of relief, such as at the base of the Saumons Sequence at Anse Mauvaise and Baie Prinsta, where underlying inner ramp facies were subject to a prolonged period of subaerial weathering and erosion (Fig. 10). Evidence of meteoric alteration at these surfaces is indicated by microkarst, with surfaces that are sharp, pitted, and stained by iron-oxides, and in updip exposures underlain by irregular pockets and cavities (Pope and Read, 1998; Hillgaertner, 1998; Brady and Bowie, 2017). Gravitational cements, solution-enlarged vugs (Desrochers et al., 2010), and depleted carbon isotopic values below unconformities in downdip settings are also suggestive of meteoric alteration (Fig. 6). Depleted carbon isotopic values are attributed to exchange with meteoric pore waters depleted in $\delta^{13}C$, given their localized expression (see Mauviel and Desrochers, 2016) and the restricted stratigraphic interval over which they occur (Allan and Matthews, 1982; Driese et al., 1994). Rare samples of intraclast breccias also have been recovered from slumps of the Ellis Bay Formation close to the Mauvaisen unconformity at Rivière Schmitt. While the stratigraphic position of these samples cannot be further constrained, their characteristics suggest a paleokarst origin.

Comparisons with Previous Sequence Stratigraphic Frameworks

Desrochers et al. (2010) is the only other study that reported unconformities from the eastern Ellis Bay Formation. In their study of the uppermost Vaureal, Ellis Bay, and lowermost Becscie formations at Anse Mauvaise, Desrochers et al. (2010) documented five T–R sequences (TR-1 through TR-5) defined by maximum regressive surfaces and subaerial unconformities, following Embry and Johannessen (1992). Desrochers et al. (2010) heavily relied on the context and

Figure 10. Photographs of the upper Mauvaisen and Saumons sequence. (A) Erosive base of the laminated shallow subtidal facies (Mss4) at the top of the Mauvaisen Sequence at Rivière aux Saumons, overlying micritic deep subtidal facies (Mds2). (B) Laminated shallow subtidal facies (Mss4) as exposed up-river from Baie Prinsta at the top of the Mauvaisen Sequence, capped by a sharp, irregular surface that marks the Saumons subaerial unconformity (SU). (C) Irregular karst surface truncating Mss4 up-river from Baie Prinsta, filled in by the lowermost inner ramp facies Cir1, which marks the base of the Saumons Sequence. (D) The contact between Mss4 and Cir1 marks the unconformity at the base of the Saumons Sequence at Anse Mauvaise; across much of the exposure at this exposure, Mss4 has been completely eroded away and is present only as rip-up clasts and as the cores of oncoids in the base of Cir1. (E) Bedding-plane view of the contact between the Saumons and Mauvaisen sequences depicted in part C up-river from Baie Prinsta, revealing an irregular karst surface that cuts down into the top of the Mauvaisen Sequence. (F) Contact between the Mauvaisen and Saumons sequences at Rivière aux Saumons showing irregular high-amplitude, low-relief undulations. (G) Bioherms of the patch reef complex facies (Cpr) in the Saumons Sequence at Rivière aux Saumons (Nine-Mile Pool exposure) are up to 4 m high and 20 m across. (H) Trough cross-bedding of coarse-grained sandstone at Rivière Natiscotec indicates the existence of dunes migrating across the inner ramp during the early stages of transgression during the Saumons Sequence.
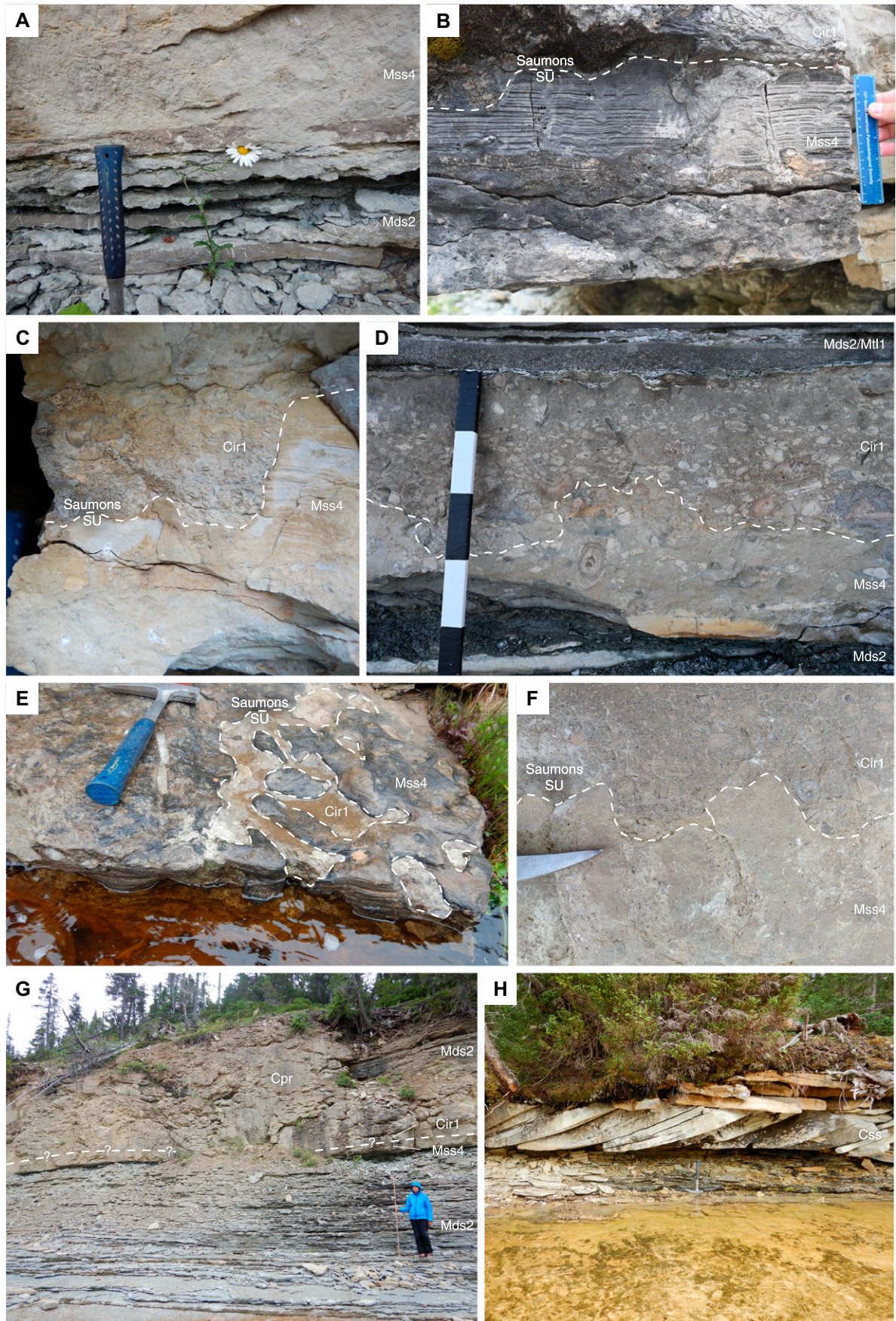
geometry of stratigraphic surfaces to infer the presence of subaerial weathering and exposure, making the inference of subaerial unconformities difficult, as many of these surfaces were modified by transgressive ravinement. In many cases, the interpretation of subaerial exposure was not substantiated until the present study. Investigation of the eastern Ellis Bay Formation westward of Anse Mauvaise demonstrates that the lateral extent of subaerial unconformities is much greater than reported by Desrochers et al. (2010); each of the subaerial unconformities at Anse Mauvaise described by Desrochers et al. (2010) can be traced westward to Rivière Natiscotec.

Differences in the criteria used to recognize and interpret major stratigraphic surfaces within the Ellis Bay Formation prevent a reconciliation between the interpretation of Desrochers et al. (2010) and the present study. For example, the Prinstan, Macairen, and Ballan depositional sequences of this study were not described by Desrochers et al. (2010), who considered them "smaller scale" parasequences within their TR-1 sequence and proposed that they had limited potential for regional correlation (Fig. 4; Desrochers et al., 2010). As shown here, the Prinstan, Macairen, and Ballan depositional sequences and their bounding surfaces are all traceable across localities of the eastern Ellis Bay Formation. Higher in the eastern Ellis Bay Formation, the maximum regressive surface separating TR-3 and TR-4 is placed at a phosphatic hardground, which is interpreted here as the maximum flooding surface of the Mauvaisen Sequence. However, these T–R sequences and the hardground separating them are not traceable west of Anse Mauvaise. Three of the five T–R sequences identified by Desrochers et al. (2010) therefore have limited potential for correlation and do not have an equivalent in the present study. Finally, the top of TR-5 lacks definitive evidence of subaerial weathering and erosion. A step-function in the upper HICE across the top of TR-5 in the western Ellis Bay Formation, used as evidence of subaerial exposure, is not present in the eastern Ellis Bay Formation, which suggests that the magnitude of the hiatus across this surface is greater in distal ramp settings than in proximal ramp settings. Therefore, either the correlation of this surface by Desrochers et al. (2010) is incorrect or the top of TR-5 is not a subaerial unconformity.

Despite these differences, some of the surfaces of Desrochers et al. (2010) coincide with surfaces identified in this study. Specifically, the base of TR-1 coincides with the base of the Prinstan Sequence, the base of TR-2 is equivalent to the base of the Natiscotecan Sequence, and the base of TR-3 is the same as the base of the Mauvaisen Sequence, which is equivalent to the entirety of both TR-3 and TR-4. Finally, the base of the TR-5 sequence coincides with the base of the Saumons Sequence, which, based on biostratigraphic and chemostratigraphic data, is the only surface that can be confidently extended to the western Ellis Bay Formation. This suggests that the Saumons unconformity is a regionally traceable surface that represents a greater fall in relative sea level compared to older unconformities in the eastern Ellis Bay Formation.

Depositional Sequences of the Ellis Bay Formation Reflect Glacioeustasy

Sequence stratigraphic architecture of Ordovician/Silurian boundary exposures is commonly interpreted to reflect an overarching glacioeustatic control on relative sea level, particularly given the climatic context of the Hirnantian Stage (Brenchley et al., 1994; Page et al., 2007; Finnegan et al., 2011). Many features of the eastern Ellis Bay Formation are consistent with a strong glacioeustatic forcing. Sequences of the eastern Ellis Bay Formation are similar to fourth-order sequences developed during the late Paleozoic and Cenozoic icehouses, being thin, on the order of 10 m or less, and incomplete at the systems tract level, (Kidwell, 1997; Read, 1998; Fielding et al., 2006; Di Celma and Cantalamessa, 2007). The overall architecture of Ellis Bay depositional sequences consists of shallowing-upward sequences of a similar magnitude bounded by closely spaced, regionally traceable unconformities. These patterns are consistent with a glacioeustatic driver of relative sea-level change (Catuneanu and Zecchin, 2013). Facies deposited during Ellis Bay TSTs and HSTs are predominantly carbonate, while facies of Ellis Bay FSSTs and LSTs reflect the influence of a nearshore siliciclastic system. This pattern of reciprocal sedimentation (Van Siclen, 1964), the "lower carbonate–upper siliciclastic" pattern of Catuneanu et al. (2011), has been attributed to high-frequency relative sea-level changes during icehouse intervals (Read, 1998). In contrast to late Paleozoic and Cenozoic sequences, the eastern Ellis Bay Formation is dominated by aggradational, progradational, and degradational stacking patterns, which are referred to as the R-cycle by Zecchin (2007). Sequences deposited during icehouse intervals are dominated by retrogradational stacking and top-truncation owing to the magnitude of transgressive ravinement associated with transgression during icehouse climates that removes much of the HST and FSST. These kinds of sequences were termed the T-cycle by Zecchin (2007). The dominance of regressive facies in the Ellis Bay Formation may reflect its development on a relatively rapidly subsiding area (see discussion of Long, 2007, in the following paragraph) in contrast to the much lower accommodation rates of other Paleozoic and Cenozoic platforms. Rapid subsidence rates would favor rapid relative sea-level rise during transgression and prevent significant truncation of regressive deposits during relative sea-level fall associated with normal and forced regression.

Alternative drivers of accommodation change, such as tectonic subsidence, would have been unlikely to generate the regular, high-frequency sequences of the Ellis Bay Formation, although subsidence rates would have modified the architecture of these depositional sequences as stated above. Backstripping analysis of Anticosti Island by Long (2007) demonstrated that rates of relative sea-level change peaked during the deposition of the Vaureal Formation and abruptly declined during the deposition of the Ellis Bay Formation. In his analysis, Long (2007) did not account for the rate of eustatic sea-level change, and therefore calculated the rate of relative sea-level (accommodation) change throughout the succession, not the rate of tectonic subsidence (e.g., Hayden et al., 2008). The onset of glacioeustatic fall during the Hirnantian would have reduced the rate of relative sea-level change compared to that of the underlying Katian strata, producing the marked decrease in rates Long (2007) calculated across the Vaureal/Ellis Bay formational contact. It is likely that elevated subsidence rates persisted or gradually declined throughout the deposition of the Ellis Bay Formation, producing a slower but overall net positive rate of relative sea-level change during the Hirnantian. Elevated rates of subsidence would have modified the relative sea-level curve for the ramp by generating rapid rises in relative sea level and prolonged periods of positive accommodation rates relative to other coeval exposures, resulting in the development of the R-cycle architecture that characterizes the Ellis Bay Formation compared to the T-cycle architecture that typifies other icehouse climates (Catuneanu and Zecchin, 2013).

Recent reappraisals of the biostratigraphy (Melchin, 2008; Achab et al., 2011, 2013; Copper et al., 2013; Copper and Jin, 2017; Zimmt and Jin, 2023) and chemostratigraphy (Mauviel and Desrochers, 2016) of the Ellis Bay Formation assigned the entire Ellis Bay (sensu Copper et al., 2013) and lowermost Becscie formations on eastern Anticosti Island to the Hirnantian Stage, implying that the six sequences described here span an interval of ~2 m.y. (Goldman et al., 2020). If time is apportioned equally among the six sequences, each sequence would represent ~333 k.y., which is close to the periodicity of the Milankovitch 400 k.y. eccentricity cycle. If

the hiatuses at each subaerial unconformity are long, as interpreted here, then the amount of time represented by the total thickness of each sequence would be substantially shorter. In their cyclostratigraphic assessment of the Ordovician/Silurian boundary on Anticosti Island, Mauviel et al. (2020) defined multiple orders of T–R cycles throughout the western Ellis Bay Formation based on bed thickness, facies transitions, and storm proximity trends, following Sami and Desrochers (1992) and Long (2007). While there potentially is evidence to suggest multiple orders of sea-level fluctuation within the eastern Ellis Bay Formation (e.g., the maximum regressive surface at the base of the Ballan Sequence), meter-scale cycles that are present in the western Ellis Bay Formation are absent from the eastern Ellis Bay Formation. Any change in relative sea level would be more apparent in the shallower water, more shoreline-proximal setting of the eastern Ellis Bay Formation, where facies transitions are more marked than in the deeper-water facies of the western Ellis Bay Formation. Given the absence of such cycles from the eastern Ellis Bay Formation, it is likely that any evidence of such meter-scale cycles within individual facies, if indeed driven by allocyclic forcing, was removed by amalgamation and scour surfaces that characterize the shallow-water facies of the eastern Ellis Bay Formation.

A comparison of the basinward extent of unconformities in the Ellis Bay Formation can be used to assess the relative magnitude of each sea-level cycle, following Desrochers et al. (2010). Unconformities present in the eastern Ellis Bay Formation are traceable across the study area, with only the base of the Ballan Sequence being marked by a maximum regressive surface, thus suggesting that the sequence-bounding unconformity may be restricted to portions of the ramp farther updip, eastward of the study area. Correlation of the unconformity at the base of the Saumons Sequence with the base of the TR-5 Sequence from Desrochers et al. (2010) extends the Saumons unconformity across the outcrop belt. This makes it the only recognized basin-wide unconformity in the Ellis Bay Formation, and therefore it represents the largest fall in relative sea level among the six sequences. Enrichments in oxygen isotopic values and cooler clumped isotopic paleotemperatures above the Saumons unconformity in the western Ellis Bay Formation support the interpretation that the surface represents the largest glacioeustatic fall during the Hirnantian Glacial Maximum (Finnegan et al., 2011; Mauviel et al., 2020). The interpreted pattern of glacioeustatic sea-level change from the Ellis Bay Formation is therefore a series of small- to moderate-amplitude, early- to mid-Hirnantian cycles that

culminated in a final, high-amplitude cycle during the mid- to late Hirnantian, followed by a rapid rise in eustatic sea level that persisted into the Rhuddanian. This is consistent with the pattern of relative sea-level fluctuations recorded in other Hirnantian exposures around the world (Ghienne et al., 2014; Kiipli and Kiipli, 2020; Calner et al., 2021).

Implications for Latest Ordovician Events

In contrast to earlier models of either one or two glacioeustatic sea drawdowns during the Hirnantian (Brenchley et al., 1994; Finney et al., 1999; Sutcliffe et al., 2000; Sheehan, 2001), the Ellis Bay Formation supports the existence of a Cenozoic-style icehouse that culminated in a middle–late Hirnantian glacial maximum. This pattern is consistent with modeling and field studies that have built an increasingly complex picture of the dynamics of glacial–interglacial cycles throughout the early Paleozoic Icehouse (Moreau, 2011; Ghienne et al., 2014; Pohl et al., 2016; Pohl and Austermann, 2018; Sinnesael et al., 2021). Because of this complexity, interbasinal correlation of sequences from different settings, particularly between ice-distal and ice-proximal sites, is tenuous at best and difficult to test with alternative correlation methods (Pohl and Austermann, 2018; Creveling et al., 2018), although interbasinal correlations of Ordovician/Silurian boundary sections have been proposed previously (e.g., Bergström et al., 2006; Melchin et al., 2013; Ghienne et al., 2014). Because of the recognized difficulties in interbasinal correlation during the Hirnantian Stage and the current limitations of biostratigraphic correlation of the Anticosti Basin with other Ordovician/Silurian boundary sections, we do not presently speculate on interbasinal correlations using the sequence stratigraphic framework for Anticosti Island.

Recent revisions to the stratigraphy of Ordovician/Silurian boundary exposures document fewer sequences (two to four) and unconformities (two to three) in Hirnantian strata (Moreau, 2011; Ghienne et al., 2014; Kiipli and Kiipli, 2020; Calner et al., 2021) compared with the six sequences and four unconformities described here for the eastern Ellis Bay Formation. Continued subsidence into the Hirnantian on Anticosti Island would have favored the preservation of sequences and their bounding surfaces compared to cratonic settings (Elrick and Read, 1991; Wilkinson et al., 1991; Brady, 2015), where evidence of subaerial weathering and exposure (e.g., karst, incision, terrestrial deposits) reflect longer periods of emergence (Pope and Read, 1998; Brenchley et al., 2006; Bergström et al., 2012; Kröger et al., 2015). Given the conditions that contributed to the excep-

tional preservation of the Ordovician/Silurian boundary on Anticosti Island, it is possible that other Ordovician/Silurian boundary exposures may be missing some of the fourth-order sea-level cycles (100–400 k.y.) recognized in this study. Alternatively, it is also possible that other Ordovician/Silurian boundary exposures record similarly subtle unconformities, particularly in stratigraphically thin sections that traditionally have been regarded as stratigraphically complete (e.g., Chen et al., 2006). This makes correlation of Hirnantian sections based on unconformities and the interpretation of stratigraphic architecture problematic, a conclusion that is further indicated by the need to now reassess the interbasinal correlations of Ghienne et al. (2014) that were based on a previous sequence stratigraphic framework for Anticosti Island by Desrochers et al. (2010). These findings, along with those from modeling studies of carbonate platform stratigraphy under icehouse conditions, remain a major challenge for the long-distance correlation of depositional sequences, particularly in the absence of supporting evidence (Read et al., 1991).

Improving our understanding of the pattern and timing of climatic and oceanographic events during the Hirnantian Stage is critical for evaluating the causes of the Late Ordovician mass extinction and understanding the subsequent pattern of recovery following the extinction event. An increasing appreciation for the complexity of climatic and oceanographic change during the Hirnantian Stage has resulted in the traditional two-pulse, climate-driven paradigm of the Late Ordovician mass extinction being called into question (Holland and Patzkowsky, 2015; Sheets et al., 2016; Wang et al., 2019). In the past decade, a range of alternative patterns and mechanisms for the extinction event have been proposed, ranging from a single event driven by mass volcanism (Jones et al., 2017; Bond and Grasby, 2020) to a prolonged event driven by environmental degradation throughout the entire Hirnantian Stage as glacial cycles intensified (Harper et al., 2014; Holland and Patzkowsky, 2015; Sheets et al., 2016). However, evaluation of these hypotheses can only be accomplished through an assessment of patterns of last occurrences in the fossil record and their relationship to geochemical proxy data of environmental and climatic change (Holland, 2020). Critically, modeling and field studies have demonstrated that patterns of last occurrences are controlled by the structure of the stratigraphic record, such that changes in relative sea level, local environment, and sedimentation rate can all influence the interpretation of the pattern and drivers of a mass extinction event (Holland, 1995; Holland and Patzkowsky, 1999; Scarponi

and Kowalewski, 2004; Nawrot et al., 2018). High-frequency glacioeustatic fluctuations throughout the Hirnantian Stage would have played an important role in the expression of the Late Ordovician mass extinction in the fossil record, even if the extinction event itself were unrelated to climatic change (Holland and Patzkowsky, 2015). Recent work has highlighted that basin-wide sequence stratigraphic frameworks are one of the only reliable means for determining the underlying pattern, timing, and tempo of a mass extinction event (Zimmt et al., 2021). An improved understanding of the stratigraphic architecture of the eastern Ellis Bay Formation at a regional scale therefore represents an important step toward the ongoing reassessment of faunal turnover across the Ordovician/Silurian boundary, particularly given that previous interpretations of faunal turnover were framed within a now-outdated lithostratigraphic framework (e.g., Copper, 2001).

CONCLUSIONS

(1) Upper Ordovician strata of the eastern Ellis Bay and lowermost Becscie formations on Anticosti Island preserve six fourth-order (∼100–400 k.y.) depositional sequences: the Prinstan, Macairen, Ballan, Natiscotecan, Mauvaisen, and Saumons sequences. These sequences record deposition in tidal, mixed carbonate–siliciclastic ramp, and carbonate ramp depositional systems, reflecting an array of environments from offshore to inner ramp and shoreface settings.

(2) Unconformities within the eastern Ellis Bay Formation are often cryptic in outcrop but are mantled by horizons of quartz pebbles that were reworked into overlying transgressive lag facies. These quartz pebble lags are the remnants of a siliciclastic system that distributed coarser clastic material across the inner and mid-ramp during the falling stage systems tract and lowstand systems tract: they are the most conspicuous features associated with subaerial weathering and erosion and can be found across the eastern Ellis Bay Formation. Similar quartz pebble lags in other mixed carbonate–siliciclastic successions may provide useful markers that indicate a period of subaerial weathering and erosion when unconformities are otherwise cryptic.

(3) Incised valley systems characterized by tidally influenced and predominantly siliciclastic facies are present within the eastern Ellis Bay Formation and indicate a drop in relative sea level of at least ∼15 m by the end of the Prinstan Sequence. The presence of these tidally influenced siliciclastic facies in eastern updip localities contrasts with their absence in western downdip exposures. Additional field study

is needed to establish the areal limits and thicknesses of these incised valley deposits.

(4) Depositional sequences of the Ellis Bay Formation are characterized by thin, truncated cycles of a similar magnitude that are bounded by regionally traceable unconformities. These features indicate a dominant glacioeustatic control on their architecture. Analysis of previous studies suggests that subsidence persisting into the Hirnantian Stage enabled the preservation of these depositional sequences and their corresponding unconformities.

(5) Comparison of the Ellis Bay Formation to coeval Hirnantian exposures suggests that other regions may be incomplete at the level of the fourth-order cycles that occur in the Ellis Bay Formation. At a regional scale, stratigraphic architecture is expected to be an overarching control on the expression of oceanographic, climatic, and biotic events, which complicates the interpretation of the pattern and drivers of the Late Ordovician mass extinction. Resulting uncertainties in interbasinal correlations based on unconformities and interpretations of stratigraphic architecture thus complicate global correlation of Hirnantian records and our understanding of the Late Ordovician mass extinction.

REFERENCES CITED

Achab, A., Asselin, E., Desrochers, A., Riva, J.F., and Farley, C., 2011, Chitinozoan contribution to the development of a new Upper Ordovician stratigraphic framework for Anticosti Island: Geological Society of America Bulletin, v. 123, p. 186–205, https://doi.org/10.1130/B30131.1.

Achab, A., Asselin, E., Desrochers, A., and Riva, J.F., 2013, The end-Ordovician chitinozoan zones of Anticosti Island, Québec: Definition and stratigraphic position: Review of Palaeobotany and Palynology, v. 198, p. 92–109, https://doi.org/10.1016/j.revpalbo.2012.07.019.

Aigner, T., 1982, Calcareous tempestites: Storm-dominated stratification in upper Muschelkalk Limestone (Middle Trias, SW-Germany), in Einsele, G., and Seilacher, A., eds., Cyclic and Event Stratification: New York, Hei-

delberg, Berlin, Springer-Verlag, p. 180–198, https://doi.org/10.1007/978-3-642-75829-4_13.

Allan, J.R., and Matthews, R.K., 1982, Isotope signatures associated with early meteoric diagenesis: Sedimentology, v. 29, p. 797–817, https://doi.org/10.1111/j.1365-3091.1982.tb00085.x.

Bambach, R.K., 1988, The Ordovician–Silurian unconformity in Western Virginia and adjacent West Virginia: Appalachian Basin Industrial Associates, v. 14, p. 1–8.

Bartlett, R., Elrick, M., Wheeley, J.R., Polyak, V., Desrochers, A., and Asmerom, Y., 2018, Abrupt global-ocean anoxia during the Late Ordovician–Early Silurian detected using uranium isotopes of marine carbonates: Proceedings of the National Academy of Sciences of the United States of America, v. 115, p. 5896–5901, https://doi.org/10.1073/pnas.1802438115.

Bergström, S.M., Saltzman, M.R., and Schmitz, B., 2006, First record of the Hirnantian (Upper Ordovician) δ13C excursion in the North American Midcontinent and its regional implications: Geological Magazine, v. 143, p. 657–678, https://doi.org/10.1017/S0016756806002469.

Bergström, S.M., Kleffner, M., and Schmitz, B., 2012, Late Ordovician–Early Silurian δ13C chemostratigraphy in the Upper Mississippi Valley: Implications for chronostratigraphy and depositional interpretations: Earth and Environmental Science Transactions of the Royal Society of Edinburgh, v. 102, p. 159–178, https://doi.org/10.1017/S1755691012011061.

Bhattacharya, J.P., 2011, Practical problems in the application of the sequence stratigraphic method and key surfaces: Integrating observations from ancient fluvial–deltaic wedges with Quaternary and modelling studies: Sedimentology, v. 58, p. 120–169, https://doi.org/10.1111/j.1365-3091.2010.01205.x.

Blakey, R.C., 1984, Marine sand-wave complex in the Permian of central Arizona: Journal of Sedimentary Petrology, v. 54, p. 29–51.

Bolton, T.E., 1972, Geological Map (22H, 12E, F) and Notes on the Ordovician and Silurian Litho- and Biostratigraphy, Anticosti Island, Quebec: Geological Survey of Canada Paper 71, no. 19, p. 1–45.

Bond, D.P.G., and Grasby, S.E., 2020, Late Ordovician mass extinction caused by volcanism, warming, and anoxia, not cooling and glaciation: Geology, v. 48, p. 777–781, https://doi.org/10.1130/G47377.1.

Bordet, E., Malo, M., and Kirkwood, D., 2010, A structural study of western Anticosti Island, St. Lawrence platform, Québec: A fracture analysis that integrates surface and subsurface structural data: Bulletin of Canadian Petroleum Geology, v. 58, p. 36–55, https://doi.org/10.2113/gscpgbull.58.1.36.

Brady, M., and Bowie, C., 2017, Discontinuity surfaces and microfacies in a storm-dominated shallow epeiric sea, Devonian Cedar Valley Group, Iowa: The Depositional Record: The Journal of the International Association of Sedimentologists, v. 3, p. 136–160, https://doi.org/10.1002/dep2.26.

Brady, M.E., 2015, Stratigraphic completeness of carbonate dominated records from continental interiors versus continental margins: Stratigraphic thinning occurs via condensation and omission at multiple scales: Journal of Sedimentary Research, v. 85, p. 337–360, https://doi.org/10.2110/jsr.2015.22.

Brenchley, P.J., Marshall, J.D., Carden, G.A.F., Robertson, D.B.R., Long, D.G.F., Meidla, T., Hints, L., and Anderson, T.F., 1994, Bathymetric and isotopic evidence for a short-lived Late Ordovician glaciation in a greenhouse period: Geology, v. 22, p. 295–298, https://doi.org/10.1130/0091-7613(1994)022<0295:BAIEFA>2.3.CO;2.

Brenchley, P.J., Marshall, J.D., Harper, D.A.T., Buttler, C.J., and Underwood, C.J., 2006, A late Ordovician (Hirnantian) karstic surface in a submarine channel, recording glacio-eustatic sea-level changes: Meifod, central Wales: Geological Journal, v. 41, p. 1–22, https://doi.org/10.1002/gj.1029.

Budd, D., Gaswirth, S., and Oliver, W.L., 2002, Quantification of macroscopic subaerial exposure features in carbonate rocks: Journal of Sedimentary Research, v. 72, p. 917–928, https://doi.org/10.1306/050502720917.

Calner, M., Bockelie, J.F., Rasmussen, C.M.Ø., Calner, H., Lehnert, O., and Joachimski, M.M., 2021, Car-

bon isotope chemostratigraphy and sea-level history of the Hirnantian Stage (uppermost Ordovician) in the Oslo–Asker district, Norway: Geological Magazine, v. 158, p. 1977–2008, https://doi.org/10.1017/S0016756821000546.

Castonguay, S., Wilson, R.A., Brisebois, D., Desrochers, A., and Malo, M., 2005, Compilation géologique, Anticosti-Gaspé-Campbellton, les ponts géologiques de l'est du Canada, Transect 4, Québec-Nouveau-Brunswick: Commission Géologique du Canada, Open File 4883, scale 1:125,000, 4 sheets.

Cattaneo, A., and Steel, R.J., 2003, Transgressive deposits: A review of their variability: Earth-Science Reviews, v. 62, p. 187–228, https://doi.org/10.1016/S0012-8252(02)00134-4.

Catuneanu, O., 2006, Principles of Sequence Stratigraphy: New York, Elsevier, 375 p.

Catuneanu, O., and Zecchin, M., 2013, High-resolution sequence stratigraphy of clastic shelves II: Controls on sequence development: Marine and Petroleum Geology, v. 39, p. 26–38, https://doi.org/10.1016/j.marpetgeo.2012.08.010.

Catuneanu, O., et al., 2009, Towards the standardization of sequence stratigraphy: Earth-Science Reviews, v. 92, p. 1–33, https://doi.org/10.1016/j.earscirev.2008.10.003.

Catuneanu, O., Galloway, W.E., Kendall, C.G.St.C., Miall, A.D., Posamentier, H.W., Strasser, A., and Tucker, M.E., 2011, Sequence stratigraphy: Methodology and nomenclature: Newsletters on Stratigraphy, v. 44, p. 173–245, https://doi.org/10.1127/0078-0421/2011/0011.

Chen, X., Rong, J.-Y., Fan, J.-X., Zhan, R.-B., Mitchell, C.E., Harper, D.A.T., Melchin, M., Peng, P., Finney, S.C., and Wang, X.-F., 2006, The Global Boundary Stratotype Section and Point (GSSP) for the base of the Hirnantian Stage (the uppermost of the Ordovician System): Episodes, v. 29, p. 183–196, https://doi.org/10.18814/epiiugs/2006/v29i3/004.

Clifton, H., 2006, A Reexamination of Facies Models for Clastic Shorelines: SEPM (Society for Sedimentary Geology) Special Publication 84, p. 293–337.

Cocks, L.R.M., and Torsvik, T.H., 2021, Ordovician palaeogeography and climate change: Gondwana Research, v. 100, p. 53–72, https://doi.org/10.1016/j.gr.2020.09.008.

Copper, P., 2001, Reefs during the multiple crises towards the Ordovician–Silurian boundary: Anticosti Island, eastern Canada, and world-wide: Canadian Journal of Earth Sciences, v. 38, p. 153–171, https://doi.org/10.1139/e00-071.

Copper, P., and Jin, J., 2014, The revised Lower Silurian (Rhuddanian) Becscie Formation, Anticosti Island, eastern Canada records the tropical marine faunal recovery from the end-Ordovician Mass Extinction: Newsletters on Stratigraphy, v. 47, p. 61–83, https://doi.org/10.1127/0078-0421/2014/0040.

Copper, P., and Jin, J., 2015, Tracking the Early Silurian post-extinction faunal recovery in the Jupiter Formation of Anticosti Island, eastern Canada: A stratigraphic revision: Newsletters on Stratigraphy, v. 48, p. 221–240, https://doi.org/10.1127/nos/2015/0061.

Copper, P., and Jin, J., 2017, Early athyride brachiopod evolution through the Ordovician–Silurian mass extinction and recovery, Anticosti Island, eastern Canada: Journal of Paleontology, v. 91, p. 1123–1147, https://doi.org/10.1017/jpa.2017.74.

Copper, P., and Long, D.G.F., 1988, Stratigraphic revisions for a key Ordovician/Silurian boundary section, Anticosti Island, Canada: Newsletters on Stratigraphy, v. 21, p. 59–73, https://doi.org/10.1127/nos/21/1989/59.

Copper, P., Long, D.G.F., and Jin, J., 2012, The Early Silurian Gun River Formation of Anticosti Island, eastern Canada: A key section for the mid-Llandovery of North America: Newsletters on Stratigraphy, v. 45, p. 263–280, https://doi.org/10.1127/0078-0421/2012/0024.

Copper, P., Jin, J., and Desrochers, A., 2013, The Ordovician–Silurian boundary (late Katian–Hirnantian) of western Anticosti Island: Revised stratigraphy and benthic megafaunal correlations: Stratigraphy, v. 10, p. 213–227, https://doi.org/10.29041/strat.10.4.02.

Creveling, J.R., Finnegan, S., Mitrovica, J.X., and Bergmann, K.D., 2018, Spatial variation in Late Ordovician gla-

cioeustatic sea-level change: Earth and Planetary Science Letters, v. 496, p. 1–9, https://doi.org/10.1016/j.epsl.2018.05.008.

Dalrymple, R.W., 2010, Tidal depositional systems, *in* James, N.P., and Dalrymple, R.W., eds., Facies Models 4: St. Johns, Newfoundland, and Labrador, Geological Association of Canada, p. 201–231.

Desrochers, A., and Gauthier, É., 2009, Carte géologique de l'île d'Anticosti (1/250,000): Ministère des Ressources naturelles et de la Faune du Québec (DV 2009-03), scale 1:250,000, 1 sheet.

Desrochers, A., Farley, C., Achab, A., Asselin, E., and Riva, J.F., 2010, A far-field record of the end Ordovician glaciation: The Ellis Bay Formation, Anticosti Island, Eastern Canada: Palaeogeography, Palaeoclimatology, Palaeoecology, v. 296, p. 248–263, https://doi.org/10.1016/j.palaeo.2010.02.017.

Di Celma, C., and Cantalamessa, G., 2007, Sedimentology and high-frequency sequence stratigraphy of a forearc extensional basin: The Miocene Caleta Herradura Formation, Mejillones Peninsula, northern Chile: Sedimentary Geology, v. 198, p. 29–52, https://doi.org/10.1016/j.sedgeo.2006.11.003.

Dott, R.H., Jr., and Bourgeois, J., 1982, Hummocky stratification: Significance of its variable bedding sequences: Geological Society of America Bulletin, v. 93, p. 663–680, https://doi.org/10.1130/0016-7606(1982)93<663:HSSOIV>2.0.CO;2.

Dowsett, H.J., 1988, Diachrony of late Neogene microfossils in the southwest Pacific Ocean: Application of the graphic correlation method: Paleoceanography, v. 3, p. 209–222, https://doi.org/10.1029/PA003i002p00209.

Driese, S.G., Srinivasan, K., Mora, C.I., and Stapor, F.W., 1994, Paleoweathering of Mississippian Monteagle Limestone preceding development of a lower Chesterian transgressive systems tract and sequence boundary, middle Tennessee and northern Alabama: Geological Society of America Bulletin, v. 106, p. 866–878, https://doi.org/10.1130/0016-7606(1994)106<0866:POMMLP>2.3.CO;2.

Droser, M.L., and Bottjer, D.J., 1989, Ordovician increase in extent and depth of bioturbation: Implications for understanding early Paleozoic ecospace utilization: Geology, v. 17, p. 850–852, https://doi.org/10.1130/0091-7613(1989)017<0850:OIIEAD>2.3.CO;2.

Elrick, M., and Read, J.F., 1991, Cyclic ramp-to-basin carbonate deposits, Lower Mississippian, Wyoming and Montana: A combined field and computer modeling study: Journal of Sedimentary Research, v. 65, p. 61–79.

Embry, A., and Johannessen, E., 1992, T–R sequence stratigraphy, facies analysis and reservoir distribution in the uppermost Triassic-Lower Jurassic succession, western Sverdrup Basin, Arctic Canada, *in* Vorren, T.O., Bergsager, E., Dahl-Stamnes, O.A., Holter, E., Johansen, B., Lie, E., and Lund, T.B., eds., Arctic Geology and Petroleum Potential: Norwegian Petroleum Society Special Publication 2, p. 121–146.

Fielding, C.R., Bann, K.L., MacEachern, J.A., Tye, S.C., and Jones, B.G., 2006, Cyclicity in the nearshore marine to coastal, Lower Permian, Pebbley Beach Formation, southern Sydney Basin, Australia: A record of relative sea-level fluctuations at the close of the Late Palaeozoic Gondwanan ice age: Sedimentology, v. 53, p. 435–463, https://doi.org/10.1111/j.1365-3091.2006.00770.x.

Finnegan, S., Bergmann, K., Eiler, J.M., Jones, D.S., Fike, D.A., Eiseman, I., Hughes, N.C., Tripati, A.K., and Fischer, W.W., 2011, The magnitude and duration of Late Ordovician–Early Silurian Glaciation: Science, v. 331, p. 903–906, https://doi.org/10.1126/science.1200803.

Finnegan, S., Heim, N.A., Peters, S.E., and Fischer, W.F., 2012, Climate change and the selective signature of the Late Ordovician mass extinction: Proceedings of the National Academy of Sciences of the United States of America, v. 109, p. 6829–6834, https://doi.org/10.1073/pnas.1117039109.

Finney, S.C., Berry, W.B.N., Cooper, J.D., Ripperdan, R.L., Sweet, W.C., Jacobson, S.R., Soufiane, A., Achab, A., and Noble, P.J., 1999, Late Ordovician mass extinction: A new perspective from stratigraphic sections in central Nevada: Geology, v. 27, p. 215–218, https://doi.org

/10.1130/0091-7613(1999)027<0215:LOMEAN>2.3.CO;2.

Föllmi, K.B., 2016, Sedimentary condensation: Earth-Science Reviews, v. 152, p. 143–180, https://doi.org/10.1016/j.earscirev.2015.11.016.

García-Hidalgo, J.F., Javier, G., Segura, M., and Domínguez, C., 2007, Internal anatomy of a mixed siliciclastic–carbonate platform: The Late Cenomanian–Mid Turonian at the southern margin of the Spanish Central System: Sedimentology, v. 54, p. 1245–1271, https://doi.org/10.1111/j.1365-3091.2007.00880.x.

Ghienne, J.-F., Desrochers, A., Vandenbroucke, T.R.A., Achab, A., Asselin, E., Dabard, M.-P., Farley, C., Loi, A., Paris, F., Wickson, S., and Veizer, J., 2014, A Cenozoic-style scenario for the end-Ordovician glaciation: Nature Communications, v. 5, https://doi.org/10.1038/ncomms5485.

Goldberg, S.L., Present, T.M., Finnegan, S., and Bergmann, K.D., 2021, A high-resolution record of early Paleozoic climate: Proceedings of the National Academy of Sciences of the United States of America, v. 118, https://doi.org/10.1073/pnas.2013083118.

Goldman, D., Sadler, P., and Leslie, S.A., 2020, The Ordovician period, *in* Gradstein, F.M., Ogg, J.G., Schmitz, M.D., and Ogg, G.M., eds., Geologic Time Scale 2020: Oxford, UK, Elsevier, p. 631–694, https://doi.org/10.1016/B978-0-12-824360-2.00020-6.

Gómez, J.J., and Fernández-López, S., 1994, Condensation processes in shallow platforms: Sedimentary Geology, v. 92, p. 147–159, https://doi.org/10.1016/0037-0738(94)90103-1.

Grélaud, C., Razin, P., Homewood, P.W., and Schwab, A.M., 2006, Development of incisions on a periodically emergent carbonate platform (Natih Formation, Late Cretaceous, Oman): Journal of Sedimentary Research, v. 76, p. 647–669, https://doi.org/10.2110/jsr.2006.058.

Harper, D.A.T., Hammarlund, E.U., and Rasmussen, C.M.Ø., 2014, End Ordovician extinctions: A coincidence of causes: Gondwana Research, v. 25, p. 1294–1307, https://doi.org/10.1016/j.gr.2012.12.021.

Hayden, T., Kominz, M.A., Powars, D.S., Edwards, L.E., Miller, K.G., Browning, J.V., and Kulpecz, A.A., 2008, Impact effects and regional tectonic insights: Backstripping the Chesapeake Bay impact structure: Geology, v. 36, p. 327–330, https://doi.org/10.1130/G24408A.1.

Haynes, J.T., 1992, Reinterpretation of Rocklandian (Upper Ordovician) K-Bentonite Stratigraphy in Southwest Virginia, Southeast West Virginia, and Northeast Tennessee: Virginia Division of Mineral Resources Publication 126, p. 1–58.

Helland-Hansen, W., and Martinsen, O.J., 1996, Shoreline trajectories and sequences: Description of variable depositional-dip scenarios: Journal of Sedimentary Research, v. 66, p. 670–688.

Hillgaertner, H., 1998, Discontinuity surfaces on a shallow-marine carbonate platform (Berriasian, Valanginian, France and Switzerland): Journal of Sedimentary Research, v. 68, p. 1093–1108, https://doi.org/10.2110/jsr.68.1093.

Holland, S.M., 1995, The stratigraphic distribution of fossils: Paleobiology, v. 21, p. 92–109, https://doi.org/10.1017/S0094837300013099.

Holland, S.M., 2020, The stratigraphic expression of mass extinctions and recoveries: Annual Review of Earth and Planetary Sciences, v. 48, p. 75–97, https://doi.org/10.1146/annurev-earth-071719-054827.

Holland, S.M., and Patzkowsky, M.E., 1996, Sequence stratigraphy and long-term paleoceanographic change in the Middle and Upper Ordovician of the eastern United States, *in* Witzke, B.J., Ludvigson, G.A., and Day, J., eds., Paleozoic Sequence Stratigraphy: Views from the North American Craton: Geological Society of America Special Paper 306, p. 117–129, https://doi.org/10.1130/0-8137-2306-X.117.

Holland, S.M., and Patzkowsky, M.E., 1997, Distal orogenic effects on peripheral bulge sedimentation: Middle and Upper Ordovician of the Nashville Dome: Journal of Sedimentary Research, v. 67, p. 250–263.

Holland, S.M., and Patzkowsky, M.E., 1999, Models for simulating the fossil record: Geology, v. 27, p. 491–494, https://doi.org/10.1130/0091-7613(1999)027<0491:MFSTFR>2.3.CO;2.

Holland, S.M., and Patzkowsky, M.E., 2015, The stratigraphy of mass extinction: Palaeontology, v. 58, p. 903–924, https://doi.org/10.1111/pala.12188.

Hunt, D., and Tucker, M.E., 1992, Stranded parasequences and the forced regressive wedge systems tract: Deposition during base-level fall: Sedimentary Geology, v. 81, p. 1–9, https://doi.org/10.1016/0037-0738(92)90052-S.

Ingram, R.L., 1954, Terminology for thickness of stratification and parting units in sedimentary rocks: Geological Society of America Bulletin, v. 65, p. 937–938, https://doi.org/10.1130/0016-7606(1954)65[937:TFTTOS]2.0.CO;2.

Jin, J., and Zhan, R., 2008, Late Ordovician Orthide and Billingsellide Brachiopods from Anticosti Island, Eastern Canada: Diversity Change through Mass Extinction: Ottawa, NRC Research Press, 159 p.

Jones, D.S., Fike, D.A., Finnegan, S., Fischer, W.W., Schrag, D.P., and McCay, D., 2011, Terminal Ordovician carbon isotope stratigraphy and glacioeustatic sea-level change across Anticosti Island (Québec, Canada): Geological Society of America Bulletin, v. 123, p. 1645–1664, https://doi.org/10.1130/B30323.1.

Jones, D.S., Martini, A.M., Fike, D.A., and Kaiho, K., 2017, A volcanic trigger for the Late Ordovician mass extinction?: Mercury data from South China and Laurentia: Geology, v. 45, p. 631–634, https://doi.org/10.1130/G38940.1.

Jones, D.S., Brothers, R.W., Crüger Ahm, A.S., Slater, N., Higgins, J.A., and Fike, D.A., 2020, Sea level, carbonate mineralogy, and early diagenesis controlled δ13C records in Upper Ordovician carbonates: Geology, v. 48, p. 194–199, https://doi.org/10.1130/G46861.1.

Khetani, A., and Read, J.F., 2002, Sequence development of a mixed carbonate-siliciclastic high-relief ramp, Mississippian, Kentucky, U.S.A.: Journal of Sedimentary Research, v. 72, p. 657–672, https://doi.org/10.1306/022102720657.

Kidwell, S.M., 1997, Anatomy of extremely thin marine sequences landward of a passive-margin hinge zone: Neogene Calvert Cliffs succession, Maryland, U.S.A.: Journal of Sedimentary Research, v. 67, p. 322–340.

Kiipli, E., and Kiipli, T., 2020, Hirnantian sea-level changes in the Baltoscandian Basin, a review: Palaeogeography, Palaeoclimatology, Palaeoecology, v. 540, https://doi.org/10.1016/j.palaeo.2019.109524.

Kröger, B., Ebbestad, J.R., Lehnert, O., Ullmann, C.V., Korte, C., Frei, R., and Rasmussen, C.M.Ø., 2015, Subaerial speleothems and deep karst in central Sweden linked to Hirnantian glaciations: Journal of the Geological Society, v. 172, p. 349–356, https://doi.org/10.1144/jgs2014-071.

Li, R.Y., and Copper, P., 2006, Early Silurian (Llandovery) Orthhide Brachiopods from Anticosti Island, Eastern Canada: The O/S Extinction Recovery Fauna: Special Papers in Palaeontology 76, 80 p.

Long, D.G.F., 2007, Tempestite frequency curves: A key to Late Ordovician and Early Silurian subsidence, sea-level change and orbital forcing in the Anticosti foreland basin, Quebec, Canada: Canadian Journal of Earth Sciences, v. 44, p. 413–431, https://doi.org/10.1139/e06-099.

Long, D.G.F., and Copper, P., 1987a, Stratigraphy of the Upper Ordovician upper Vaureal and Ellis Bay formations, eastern Anticosti Island, Quebec: Canadian Journal of Earth Sciences, v. 24, p. 1807–1820, https://doi.org/10.1139/e87-172.

Long, D.G.F., and Copper, P., 1987b, Late Ordovician sandwave complexes on Anticosti Island, Quebec: A marine tidal embayment: Canadian Journal of Earth Sciences, v. 24, p. 1821–1832, https://doi.org/10.1139/e87-173.

Mauviel, A., and Desrochers, A., 2016, A high-resolution, continuous δ13C record spanning the Ordovician–Silurian boundary on Anticosti Island, eastern Canada: Canadian Journal of Earth Sciences, v. 53, p. 795–801, https://doi.org/10.1139/cjes-2016-0003.

Mauviel, A., Sinnesael, M., and Desrochers, A., 2020, The stratigraphic and geochemical imprints of Late Ordovician glaciation on far-field neritic carbonates, Anticosti Island, eastern Canada: Palaeogeography, Palaeoclimatology, Palaeoecology, v. 543, https://doi.org/10.1016/j.palaeo.2019.109579.

McCracken, A.D., and Barnes, C.R., 1981, Conodont biostratigraphy and paleoecology of the Ellis Bay Formation, Anticosti Island, Quebec, with special reference to Late Ordovician–Early Silurian chronostratigraphy and the systemic boundary: Geological Survey of Canada Bulletin, v. 329, p. 51–134, https://doi.org/10.4095/119430.

McCracken, A.D., and Nowlan, G.S., 1988, The Gamachian Stage and Fauna 13: New York State Museum Bulletin, v. 462, p. 71–79.

McLaughlin, P.I., and Brett, C.E., 2004, Eustatic and tectonic control on the distribution of marine seismites: Examples from the Upper Ordovician of Kentucky, USA: Sedimentary Geology, v. 168, p. 165–192, https://doi.org/10.1016/j.sedgeo.2004.02.005.

McLaughlin, P.I., and Brett, C.E., 2007, Signatures of sea-level rise on the carbonate margin of a Late Ordovician foreland basin: A case study from the Cincinnati Arch, USA: Palaios, v. 22, p. 245–267, https://doi.org/10.2110/palo.2006.p06-106.

Melchin, M.J., 2008, Restudy of some Ordovician–Silurian boundary graptolites from Anticosti Island, Canada, and their biostratigraphic significance: Lethaia, v. 41, p. 155–162, https://doi.org/10.1111/j.1502-3931.2007.00045.x.

Melchin, M.J., Mitchelll, C.E., Holmden, C., and Štorch, P., 2013, Environmental changes in the Late Ordovician–early Silurian: Review and new insights from black shales and nitrogen isotopes: Geological Society of America Bulletin, v. 125, p. 1635–1670, https://doi.org/10.1130/B30812.1.

Moreau, J., 2011, The Late Ordovician deglaciation sequence of the SW Murzuq Basin (Libya): Basin Research, v. 23, p. 449–477, https://doi.org/10.1111/j.1365-2117.2010.00499.x.

Myrow, P.M., Tice, L., Archuleta, B., Clark, B., Taylor, J.F., and Ripperdan, R.L., 2004, Flat-pebble conglomerate: Its multiple origins and relationship to metre-scale depositional cycles: Sedimentology, v. 51, p. 973–996, https://doi.org/10.1111/j.1365-3091.2004.00657.x.

Nawrot, R., Scarponi, D., Azzarone, M., Dexter, T.A., Kusnerik, K.M., Wittmer, J.M., Amorosi, A., and Kowalewski, M., 2018, Stratigraphic signatures of mass extinctions: Ecological and sedimentary determinants: Proceedings of the Royal Society B: Biological Sciences, v. 285, https://doi.org/10.1098/rspb.2018.1191.

Olariu, C., Steel, R.J., Dalrymple, R.W., and Gingras, M.K., 2012, Tidal dunes v. tidal bars: The sedimentological and architectural characteristics of compound dunes in a tidal seaway, the lower Baronia Sandstone (Lower Eocene), Ager Basin, Spain: Sedimentary Geology, v. 279, p. 134–155, https://doi.org/10.1016/j.sedgeo.2012.07.018.

Osleger, D.A., and Montañez, I.P., 1996, Cross-platform architecture of a sequence boundary in mixed siliciclastic–carbonate lithofacies, Middle Cambrian, southern Great Basin, USA: Sedimentology, v. 43, p. 197–217, https://doi.org/10.1046/j.1365-3091.1996.d01-13.x.

Page, A.A., Zalasiewicz, J.A., Williams, M., and Popov, L.E., 2007, Were transgressive black shales a negative feedback modulating glacioeustasy in the Early Paleozoic Icehouse, in Haywood, W.M., Gregory, A.M., and Schmidt, D.N., eds., Deep-Time Perspectives on Climate Change: Marrying the Signal from Computer Models and Biological Proxies: Geological Society, London, The Micropaleontological Society Special Publication 2, p. 123–156, https://doi.org/10.1144/TMS002.6.

Pattison, S.A.J., 1995, Sequence stratigraphic significance of sharp-based lowstand shoreface deposits, Kenilworth Member, Book Cliffs, Utah: AAPG Bulletin, v. 79, p. 444–462.

Petryk, A.A., 1981, Stratigraphy, sedimentology, and paleogeography of the Upper Ordovician–Lower Silurian of Anticosti Island Québec, in Lespérance, P.J., ed., Field Meeting: Anticosti-Gaspe, Quebec: International Union of Geological Sciences, p. 11–39.

Pinet, N., and Lavoie, D., 2007, The offshore part of the Anticosti Basin: A major gap in the understanding of early to middle Paleozoic basins of Eastern Canada in a promising hydrocarbon setting, in Convention Extended Abstracts: Calgary, Canadian Society of Petroleum Geologists, p. 336–339.

Pinet, N., Keating, P., Lavoie, D., Dietrich, J., Duchesne, M.J., and Brake, V., 2012, Revisiting the Appalachian structural front and offshore Anticosti Basin (north-ern Gulf of St. Lawrence, Canada) by integrating old and new geophysical datasets: Marine and Petroleum Geology, v. 32, p. 50–62, https://doi.org/10.1016/j.marpetgeo.2011.12.004.

Pohl, A., and Austermann, J., 2018, A sea-level fingerprint of Late-Ordovician ice sheet collapse: Geology, v. 46, p. 595–598, https://doi.org/10.1130/G40189.1.

Pohl, A., Donnadieu, Y., Le Hir, G., Ladant, J.-B., Dumas, C., Alvarez-Solas, J., and Vandenbroucke, T.R.A., 2016, Glacial onset predated Late Ordovician climate cooling: Paleoceanography, v. 31, p. 800–821, https://doi.org/10.1002/2016PA002928.

Pope, M., and Read, J.F., 1998, Ordovician metre-scale cycles: Implications for climate and eustatic fluctuations in the central Appalachians during a global greenhouse, non-glacial to glacial transition: Palaeogeography, Palaeoclimatology, Palaeoecology, v. 138, p. 27–42, https://doi.org/10.1016/S0031-0182(97)00130-2.

Railsback, L.B., Layou, K.M., Heim, N.A., Holland, S.M., Trogdon, M.L., Jarrett, M.B., Izsak, G.M., Bulger, D.E., Wysong, E.J., Trubee, K.S., Fiser, J.M., Cox, J.E., and Crowe, D.E., 2012: Geochemical evidence for meteoric diagenesis and cryptic surfaces of subaerial exposure in subtidal carbonates from the Upper Ordovician of the Nashville Dome, Central Tennessee, U.S.A., in Ketzer, M., and Morad, S., eds., Linking Diagenesis to Sequence Stratigraphy of Sedimentary Rocks: International Association of Sedimentologists Special Publication 45, p. 257–270.

Read, J.F., 1998, Phanerozoic carbonate ramps from greenhouse, transitional, and ice-house worlds: Clues from field and modelling studies, in Wright, V.P., and Burchette, T.P., eds., Carbonate Ramps: Geological Society, London, Special Publication 149, p. 107–135, https://doi.org/10.1144/GSL.SP.1999.149.01.07.

Read, J.F., and Repetski, J.E., 2012, Cambrian–lower Middle Ordovician passive carbonate margin, southern Appalachians, in Derby, J.R., Fritz, R.D., Longacre, S.A., Morgan, W.A., and Sternbach, C.A., eds., The Great American Carbonate Bank: The Geology and Economic Resources of the Cambrian—Ordovician Sauk Megasequence of Laurentia: American Association of Petroleum Geologists Memoir 98, p. 35–382, https://doi.org/10.1306/13331499M980271.

Read, J.F., Osleger, D.A., and Elric, M., 1991, Two-dimensional modeling of carbonate ramp sequences and component cycles, in Franseen, E.K., Watney, W.L., Kendall, C.G.S.C., and Ross, W., eds., Sedimentary Modeling: Computer Simulations and Methods for Improved Parameter Definition: Kansas Geological Survey Bulletin 233, p. 473–488.

Rong, J., Xu, C., and Harper, D.A.T., 2002, The latest Ordovician Hirnantia fauna (Brachiopoda) in time and space: Lethaia, v. 35, p. 231–249, https://doi.org/10.1111/j.1502-3931.2002.tb00081.x.

Rong, J., Harper, D.A.T., Huang, B., Li, R., Zhang, X., and Chen, D., 2020, The latest Ordovician Hirnantian brachiopod faunas: New global insights: Earth-Science Reviews, v. 208, https://doi.org/10.1016/j.earscirev.2020.103280.

Sami, T., and Desrochers, A., 1992, Episodic sedimentation on an Early Silurian, storm-dominated carbonate ramp, Becscie and Merrimack formations, Anticosti Island, Canada: Sedimentology, v. 39, p. 355–381, https://doi.org/10.1111/j.1365-3091.1992.tb02122.x.

Sanford, B.V., 1993, St. Lawrence Platform—Geology, in Scott, D.F., and Aitken, J.D., eds., Sedimentary Cover of the Craton in Canada: Geological Society of America, Decade of North American Geology: Geology of North America, v. D-1, p. 723–786, https://doi.org/10.1130/DNAG-GNA-D1.723.

Saylor, B.Z., 2003, Sequence stratigraphy and carbonate–siliciclastic mixing in a terminal Proterozoic foreland basin, Urusis Formation, Nama Group, Namibia: Journal of Sedimentary Research, v. 73, p. 264–279, https://doi.org/10.1306/082602730264.

Scarponi, D., and Kowalewski, M., 2004, Stratigraphic paleoecology: Bathymetric signatures and sequence overprint of mollusk associations form upper Quaternary sequences of the Po Plain, Italy: Geology, v. 32, p. 989–992, https://doi.org/10.1130/G20808.1.

Scholle, P.A., and Ulmer-Scholle, D.S., 2003, A Color Guide to the Petrography of Carbonate Rocks: Grains, Textures, Porosity, Diagenesis: Tulsa, Oklahoma, American

Association of Petroleum Geologists, 459 p., https://doi.org/10.1306/M77973.

Schuchert, C., and Twehhofel, W.H., 1910, Ordovician–Silurian section of the Mingan and Anticosti islands, Gulf of Saint Lawrence: Geological Society of America Bulletin, v. 21, p. 667–716, https://doi.org/10.1130/GSAB-21-667.

Sepkoski, J.J., 1982, Flat-pebble conglomerates, storm deposits, and the Cambrian bottom fauna, *in* Einsele, G., and Seilacher, A., eds., Cyclic and Event Stratification: Berlin, Heidelberg, Springer, p. 371–385, https://doi.org/10.1007/978-3-642-75829-4_28.

Sheehan, P.M., 2001, The Late Ordovician mass extinction: Annual Review of Earth and Planetary Sciences, v. 29, p. 331–364, https://doi.org/10.1146/annurev.earth.29.1.331.

Sheets, H.D., Mitchell, C.E., Melchin, M.J., Loxton, J., Storch, P., Carlucci, K.L., and Hawkins, A.D., 2016, Graptolite community responses to global climate change and the Late Ordovician mass extinction: Proceedings of the National Academy of Sciences of the United States of America, v. 113, p. 8380–8385, https://doi.org/10.1073/pnas.1602102113.

Sinnesael, M., McLaughlin, P.I., Desrochers, A., Mauviel, A., De Weirdt, J., Claeys, P., and Vandenbroucke, T.R.A., 2021, Precession-driven climate cycles and time scale prior to the Hirnantian glacial maximum: Geology, v. 49, p. 1295–1300, https://doi.org/10.1130/G49083.1.

Smith, L.B., Jr., and Read, J.F., 2000, Rapid onset of late Paleozoic glaciation on Gondwana: Evidence from Upper Mississippian strata of the Midcontinent, United States: Geology, v. 28, p. 279–282, https://doi.org/10.1130/0091-7613(2000)28<279:ROOLPG>2.0.CO;2.

Sutcliffe, O.E., Dowdeswell, J.A., Whittington, R.J., Theron, J.N., and Craig, J., 2000, Calibrating the Late Ordovician glaciation and mass extinction by the eccentricity cycles of Earth's orbit: Geology, v. 28, p. 967–970, https://doi.org/10.1130/0091-7613(2000)28<967:CTLOGA>2.0.CO;2.

Swanson-Hysell, N.K., and Macdonald, F.A., 2017, Tropical weathering of the Taconic orogeny as a driver for Ordovician cooling: Geology, v. 45, p. 719–722, https://doi.org/10.1130/G38985.1.

Testa, V., and Bosence, D.W.J., 1998, Carbonate–siliciclastic sedimentation on a high-energy, ocean-facing, tropical ramp, NE Brazil, *in* Wright, V.P., and Burchette, T.P., eds., Carbonate Ramps: Geological Society, London, Special Publication 149, p. 55–71, https://doi.org/10.1144/GSL.SP.1999.149.01.05.

Torsvik, T.H., and Cocks, L.R.M., 2016, Ordovician, *in* Torsvik, T.H., and Cocks, L.R.M., eds., Earth History and Palaeogeography: Cambridge, UK, Cambridge University Press, p. 101–123, https://doi.org/10.1017/9781316225523.007.

Twehhofel, W.H., et al., 1954, Correlation of the Ordovician Formations of North America: Geological Society of America Bulletin, v. 65, p. 247–298, https://doi.org/10.1130/0016-7606(1954)65[299:COTOFO]2.0.CO;2.

Vandenbroucke, T.R.A., Armstrong, H.A., Williams, M., Paris, F., Sabbe, K., Zalasiewicz, J.A., Nõlvak, J., and Verniers, J., 2010, Epipelagic chitinozoan biotopes map a steep latitudinal temperature gradient for earliest Late Ordovician seas: Implications for a cooling Late Ordovician climate: Palaeogeography, Palaeoclimatology, Palaeoecology, v. 294, p. 202–219, https://doi.org/10.1016/j.palaeo.2009.11.026.

Van Siclen, D.C., 1964, Depositional topography in relation to cyclic sedimentation, *in* Merriam, D.F., ed., Symposium on Cyclic Sedimentation: Lawrence, Kansas, Kansas Geological Survey Bulletin 169, p. 533–539.

Wang, G., Zhan, R., and Percival, I.G., 2019, The end-Ordovician mass extinction: A single-pulse event?: Earth-Science Reviews, v. 192, p. 15–33, https://doi.org/10.1016/j.earscirev.2019.01.023.

Wilkinson, B.H., Opdyke, B.N., and Algeo, T.J., 1991, Time partitioning in cratonic carbonate rocks: Geology, v. 19, p. 1093–1096, https://doi.org/10.1130/0091-7613(1991)019<1093:TPICCR>2.3.CO;2.

Wynn, T.C., and Read, J.F., 2008, Three-dimensional sequence analysis of a subsurface carbonate ramp, Mississippian Appalachian foreland basin, West Virginia, USA: Sedimentology, v. 55, p. 357–394, https://doi.org/10.1111/j.1365-3091.2007.00905.x.

Xiao, Y., Suzuki, N., and He, W., 2018, Low-latitudinal standard Permian radiolarian biostratigraphy for multiple purposes with unitary association, graphic correlation, and Bayesian inference methods: Earth-Science Reviews, v. 179, p. 168–206, https://doi.org/10.1016/j.earscirev.2018.02.011.

Zecchin, M., 2007, The architectural variability of small-scale cycles in shelf and ramp clastic systems: The controlling factors: Earth-Science Reviews, v. 84, p. 21–55, https://doi.org/10.1016/j.earscirev.2007.05.003.

Zecchin, M., and Catuneanu, O., 2013, High-resolution sequence stratigraphy of clastic shelves I: Units and bounding surfaces: Marine and Petroleum Geology, v. 39, p. 1–25, https://doi.org/10.1016/j.marpetgeo.2012.08.015.

Zecchin, M., and Catuneanu, O., 2017, High-resolution sequence stratigraphy of clastic shelves VI: Mixed siliciclastic-carbonate systems: Marine and Petroleum Geology, v. 88, p. 712–723, https://doi.org/10.1016/j.marpetgeo.2017.09.012.

Zimmt, J.B., and Jin, J., 2023, A new species of *Hirnantia* (Orthida, Brachiopoda) and its implications for the Hirnantian age of the Ellis Bay Formation, Anticosti Island, eastern Canada: Journal of Paleontology, v. 97, p. 47–62, https://doi.org/10.1017/jpa.2022.83.

Zimmt, J.B., Holland, S.M., Finnegan, S., and Marshall, C.R., 2021, Recognizing pulses of extinction from clusters of last occurrences: Palaeontology, v. 64, p. 1–20, https://doi.org/10.1111/pala.12505.

Zou, C., Qui, Z., Poulton, S.W., Dong, D., Wang, H., Chen, D., Lu, B., Shi, Z., and Tao, H., 2018, Ocean euxinia and climate change "double whammy" drove the Late Ordovician mass extinction: Geology, v. 46, p. 535–538, https://doi.org/10.1130/G40121.1.